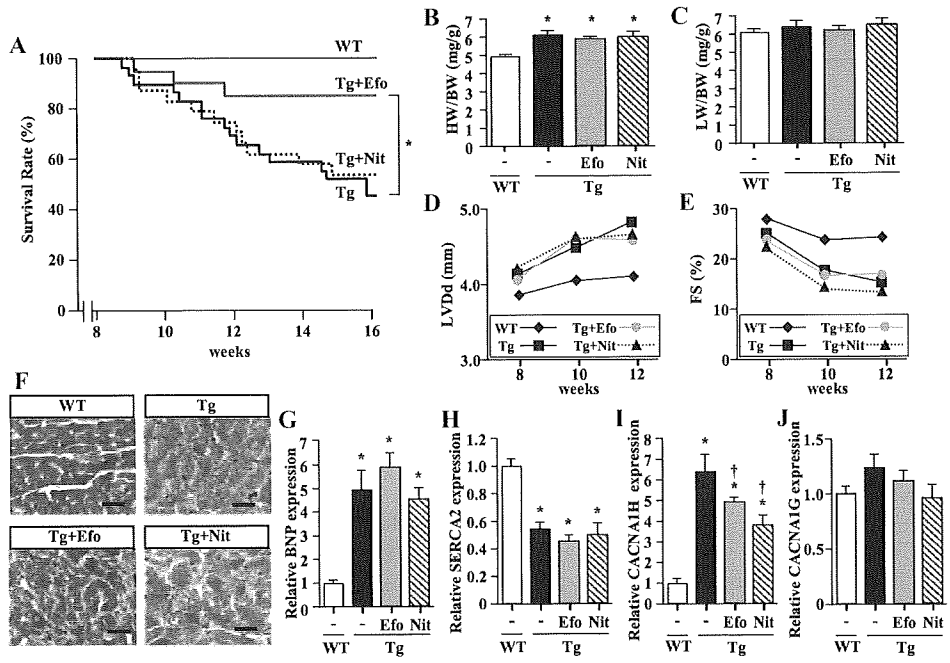

Figure 2. Efonidipine prolongs survival among dnNRSF-Tg mice. A, Kaplan-Meier survival curves for WT and dnNRSF-Tg (Tg) mice, with or without efonidipine (Efo) or nitrendipine (Nit), during the 7-week drug administration period (from 8 to 15 weeks of age). *$P<0.05$ (n=7 for WT, n=27 for Tg without drugs, n=19 for Tg with Efo, n=22 for Tg with Nit). B and C, heart weight–to–body weight (HW/BW) ratios (B) and lung weight–to–body weight (LW/BW) ratios (C) in 12-week-old WT and Tg mice, with or without Efo or Nit. *$P<0.05$ vs WT (n=10 for each group). D and E, Left ventricular diastolic dimension (LVDd; D) and % fractional shortening (FS; E), assessed echocardiographically in WT and Tg mice, with or without Efo or Nit, during a 4-week period beginning when the mice were 8 weeks of age (n=4 for WT, n=5 for Tg without drugs, n=6 for Tg with Efo, n=5 for Tg with Nit). The comparison of trends in LVDd and FS over time among Tg, Tg with Efo, and Tg with Nit, by repeated-measures analyses with linear mixed-effects models, showed no statistical significance (LVDd, $P=0.689$; FS, $P=0.735$). F, Histology of WT and dnNRSF-Tg hearts from 12-week-old mice treated with or without Efo or Nit. Hematoxylin-and-eosin staining; magnification ×400. Scale bars=20 μm. G–J, Relative levels of *BNP* (G), *SERCA2* (H), *CACNA1H* (I), and *CACNA1G* (J) mRNA expression in hearts from 12-week-old WT and Tg mice treated with or without Efo or Nit. *$P<0.05$ vs WT, †$P<0.05$ vs Tg without drugs (n=4 for WT, n=5 for Tg without drugs, n=4 for Tg with Efo, n=4 for Tg with Nit).

Results

Dual T- and L-Type Ca^{2+} Channel Blocker Efonidipine Improves Survival Among dnNRSF-Tg Mice

We previously showed that dnNRSF-Tg mice develop progressive cardiomyopathy and begin to die of ventricular tachyarrhythmias at ≈8 weeks of age.[14] In dnNRSF-Tg hearts, *CACNA1H*, the gene that encodes the T-type Ca^{2+} channel α-subunit and a transcriptional target of NRSF/REST, was upregulated, and there was a corresponding increase in $I_{Ca,T}$ amplitude in the isolated ventricular myocytes (Figure 1A through 1C).[14] By contrast, no $I_{Ca,T}$ were recorded in adult ventricular myocytes from wild-type littermate (WT) hearts (Figure 1A).[14] To determine the role played by T-type Ca^{2+} channels in the development of malignant arrhythmias and sudden death and to assess the potential therapeutic effect of T-type Ca^{2+} channel blockade in dnNRSF-Tg mice, we administered subpressor doses of efonidipine, a dual T- and L-type dihydropyridine Ca^{2+} channel blocker,[15,16] or nitrendipine, a more L-type-selective dihydropyridine Ca^{2+} channel blocker, to dnNRSF-Tg mice for 7 weeks, beginning when they were 8 weeks of age. Initially, we confirmed that efonidipine significantly blocked $I_{Ca,T}$ in ventricular myocytes from dnNRSF-Tg mice (Figure 1D and 1E). Consistent with previous reports, efonidipine also blocked $I_{Ca,L}$ in those cells (Figure 1D and 1E).[15,16] As shown in Figure 2A, efonidipine dramatically improved the survival rate among dnNRSF-Tg mice compared with mice treated with nitrendipine or control vehicle. We found that heart weight–to–body weight ratios and lung weight–to–body weight ratios did not differ among the control, efonidipine, and nitrendipine groups (Figure 2B and 2C). In addition, echocardiographic, hemodynamic, and histological analyses showed no significant differences among these 3 groups (Figure 2D, 2E, and 2F; Table). Consistent with these findings, there also was no significant difference in the expression of 2 cardiac stress marker genes, *BNP* and *SERCA2*, among the 3 groups (Figure 2G and 2H).[26,27] Both efonidipine and nitrendipine modestly reduced the increase in *CACNA1H* expression seen in dnNRSF-Tg hearts (Figure 2I), and the expression of *CACNA1G* did not significantly differ among WT and dnNRSF-Tg mice (Figure 2J). These data suggest that efonidipine directly suppresses sudden death in dnNRSF-Tg mice without significantly affecting cardiac structure or function.

Efonidipine Reduces Arrhythmogenicity in dnNRSF-Tg Mice

We next used a telemetric monitoring system to examine the effects of each drug on ECG parameters in dnNRSF-Tg mice. We found that only efonidipine significantly suppressed the

Table. Body Weight, Blood Pressure, and Hemodynamic Parameters in 12-Week-Old WT and dnNRSF-Tg Mice Treated With or Without Efonidipine or Nitrendipine

		dnNSF-Tg Mice		
	WT	Untreated	Treated With Efonidipine	Treated With Nitrendipine
Body weight, g	26.5±0.5	25.0±0.4*	24.8±0.6*	24.6±0.4*
Blood pressure, mm Hg	105.3±3.6	96.7±2.2*	94.4±3.8*	98.0±7.1*
Echocardiographic data				
LVDd, mm	4.1±0.4	4.8±0.2*	4.6±0.2*	4.6±0.2*
LVDs, mm	3.3±0.1	4.1±0.2*	3.8±0.1*	4.0±0.2*
FS, %	23.5±0.3	14.0±1.6*	17.0±0.6*	13.8±0.4*
IVS, mm	0.75±0.03	0.72±0.04	0.78±0.05	0.76±0.02
PW, mm	0.73±0.02	0.70±0.04	0.68±0.04	0.76±0.02
Hemodynamic data				
LVSP, mm Hg	112±3	107±3*	105±2*	103±3*
LVEDP, mm Hg	7.4±0.9	6.3±2.1	4.8±1.1	8.0±0.9
dP/dt, mm Hg/s	5430±150	4600±248*	4683±192*	4480±213*
−dP/dt, mm Hg/s	4400±435	3775±309	3833±158	3440±260
HR, bpm	452±39	415±20	419±36	428±26

LVDd indicates left ventricular diastolic dimension; LVDs, left ventricular systolic dimension; FS, fractional shortening; IVS, intraventricular septum wall thickness; PW, posterior wall thickness; LVSP, left ventricular systolic pressure; LVEDP, left ventricular end-diastolic pressure; and HR, heart rate.

Values are mean±SEM. Numbers of mice tested were as follows: Body weight, n=10 for each group; blood pressure, n=6 for WT mice, n=14 for dnNRSF-Tg mice without drugs, n=5 for dnNRSF-Tg mice treated with efonidipine, n=7 for dnNRSF-Tg mice treated with nitrendipine; echocardiographic data, n=4 for WT mice, n=5 for dnNRSF-Tg mice without drugs, n=6 for dnNRSF-Tg mice treated with efonidipine, n=5 for dnNRSF-Tg mice treated with nitrendipine; hemodynamic data, n=5 for WT mice, n=4 for dnNRSF-Tg mice without drugs, n=6 for dnNRSF-Tg mice treated with efonidipine, n=5 for dnNRSF-Tg mice treated with nitrendipine.

*$P<0.05$ vs WT mice.

number of premature ventricular contractions in dnNRSF-Tg hearts (Figure 3A). More importantly, it dramatically reduced the number of episodes of ventricular tachycardia (VT; Figure 3B).

We further assessed the effect of each drug on arrhythmogenicity in dnNRSF-Tg mice by performing an in vivo intracardiac electrophysiological analysis.[14,25] We found that control dnNRSF-Tg mice were highly susceptible to induction of VT, as reported previously[14] (Figure 3C and 3D), and that nitrendipine did not reduce that susceptibility (Figure 3D). By contrast, efonidipine significantly reduced the frequency of induced VT (Figure 3C and 3D). To confirm that inhibition of T-type Ca^{2+} currents is responsible for the suppression of arrhythmogenicity in dnNRSF-Tg hearts, we next treated dnNRSF-Tg mice with another dual T- and L-type Ca^{2+} channel blocker, mibefradil.[28] After 1 week of treatment with mibefradil or efonidipine, dnNRSF-Tg mice showed significantly reduced susceptibility to induced VT (Figure 3E).

We next examined the effects of long-term drug treatment on the electrophysiological properties of myocytes isolated from dnNRSF-Tg hearts. When we measured action potentials elicited in isolated ventricular myocytes from WT and dnNRSF-Tg hearts, we found that in the latter, the membrane potential was somewhat depolarized, and the action potential duration was increased (Figure 3F and 3G). Efonidipine, but not nitrendipine, significantly restored the resting membrane potential in dnNRSF-Tg myocytes (Figure 3F and 3G).

Efonidipine Improves Cardiac Autonomic Nervous System Function in dnNRSF-Tg Mice

A disturbance of autonomic nerve activity that leads to increased sympathetic nerve activity and reduced parasympathetic nerve activity is involved in the increased arrhythmogenicity seen in patients with chronic heart failure. Heart rate variability (HRV) is a widely accepted index of cardiac autonomic nervous system activity.[29] A previous frequency-domain analysis of HRV revealed that patients with severe heart failure show a progressive reduction in power in both the low-frequency and high-frequency ranges.[29,30] Moreover, the reduction in low-frequency power is a significant predictor of sudden cardiac death in patients with heart failure.[31,32]

T-type Ca^{2+} channels are normally expressed in neuronal and endocrine tissues, where they play an important role in mediating neurotransmitter release and in the secretion of various neurohumoral factors, including catecholamines.[33] Indeed, T-type Ca^{2+} channel blockade reportedly modulates autonomic activity.[34,35] With that in mind, we hypothesized that in addition to its direct effects on cardiac electrophysiological properties, T-type Ca^{2+} blockade reduces arrhythmogenicity by modulating autonomic nerve function. To test that idea, we used HRV as an index with which to evaluate cardiac autonomic function in WT and dnNRSF-Tg mice.[29] In mice, HRV predominantly correlates with parasympathetic activity.[36] Mice are nocturnal, so that for any given "day," the power in both the low- and high-frequency ranges was lower during the dark (night) phase, when the mice were more

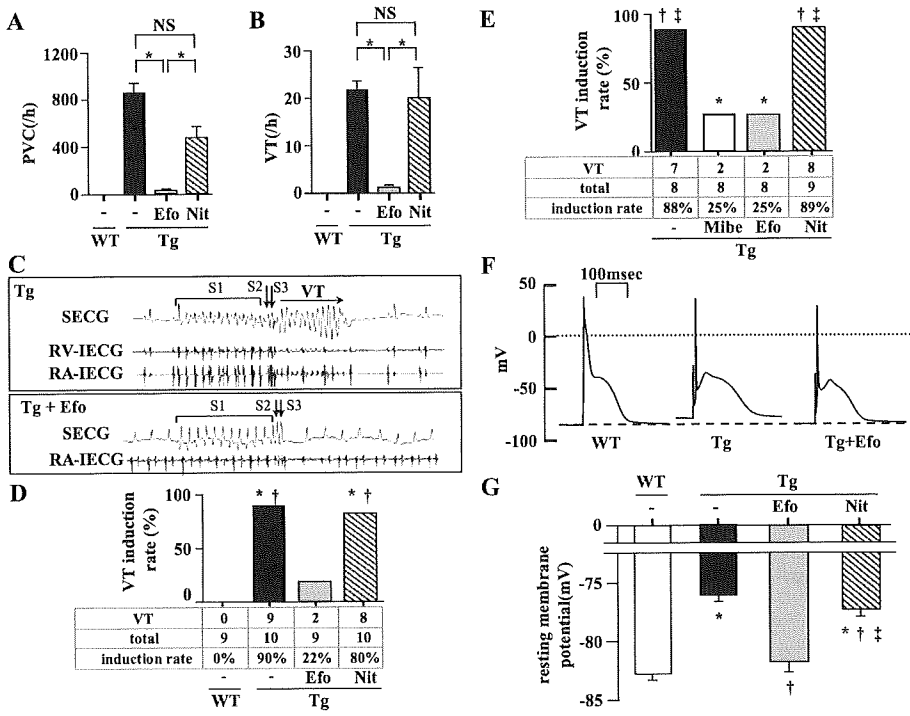

Figure 3. Efonidipine reduces arrhythmogenicity in dnNRSF-Tg hearts. A and B, Numbers of premature ventricular contractions (PVC; A) and VT (B) recorded with a telemetry system in WT and dnNRSF-Tg (Tg) mice treated with or without efonidipine (Efo) or nitrendipine (Nit). *$P<0.05$ (n=5 for WT, n=8 for Tg without drugs, n=7 for Tg with Efo, n=7 for Tg with Nit). C, Representative ECG traces from an in vivo electrophysiological study performed to evaluate the inducibility of VT in Tg hearts from mice treated with or without Efo. VT was induced in control hearts (upper panel) but not in those treated with efonidipine (Tg+Efo, lower panel). SECG indicates surface ECG; RV-IECG, intracardiac ECG (right ventricle); and RA-IECG, intracardiac ECG (right atrium). D, Frequency of mice with inducible VTs in Tg mice treated for 7 weeks with or without Efo or Nit. VT indicates number of mice with inducible VT; total, total number of mice tested. *$P<0.05$ vs WT, †$P<0.05$ vs Tg with Efo. E, Frequency of mice with inducible VTs in Tg mice treated for 1 week with or without mibefradil (Mibe), Efo, or Nit. VT indicates number of mice with inducible VT; total, total number of mice tested. *$P<0.05$ vs Tg, †$P<0.05$ vs Tg with Mibe; ‡$P<0.05$ vs Tg with Efo. F and G, Representative traces of action potentials (F) and averages of resting membrane potentials (G) recorded from isolated ventricular myocytes from 12-week-old WT and Tg mice treated with or without Efo. *$P<0.05$ vs WT, †$P<0.05$ vs control Tg, ‡$P<0.05$ vs Tg with Efo (n=12 for WT, n=12 for Tg without drugs, n=14 for Tg with Efo, n=18 for Tg with Nit).

active, than during the light (day) phase (online-only Data Supplement Figure IA and IB). In dnNRSF-Tg mice, the incidences of both premature ventricular contractions and VTs were much greater during the dark phase, which suggests the involvement of autonomic nerve activity in the generation of arrhythmias in these mice (online-only Data Supplement Figure IC and ID). In addition, the averages of both the low- and high-frequency powers over 24 hours in dnNRSF-Tg mice were markedly lower than in WT mice, which indicates a general reduction in parasympathetic activity in dnNRSF-Tg mice (Figure 4A, 4B, and 4C). Efonidipine dramatically increased the power in both the low- and high-frequency ranges of HRV in dnNRSF-Tg mice, whereas nitrendipine had little effect on HRV (Figure 4A, 4B, and 4C). We also found that urinary excretion of norepinephrine, which is indicative of the level of sympathetic nerve activity, was significantly higher in dnNRSF-Tg than in WT mice (Figure 5A). Moreover, the increased excretion of norepinephrine seen in dnNRSF-Tg mice was attenuated significantly only by efonidipine (Figure 5A).

We next evaluated the response of dnNRSF-Tg myocytes to catecholaminergic stimulation. We found that in the presence of isoproterenol 3 μmol/L, isolated ventricular myocytes from dnNRSF-Tg hearts showed early afterdepolarizations and spontaneous action potentials, whereas myocytes from WT hearts did not (Figure 5B, through 5D). In addition, systemic administration of isoproterenol induced VT more frequently in dnNRSF-Tg mice than in WT mice (Figure 5E). These data support our idea that abnormal autonomic nervous system balance, with decreased parasympathetic activity and increased sympathetic activity, facilitates arrhythmogenesis in dnNRSF-Tg mice. The increase in the frequency of isoproterenol-induced VT seen in dnNRSF-Tg mice was attenuated significantly by efonidipine but not by nitrendipine (Figure 5E). Thus, along with its direct effect, which reduces the vulnerability of the heart to arrhythmogenic stress (Figures 3D, 3E, and 5E), efonidipine also improves the cardiac autonomic nervous system balance, which further contributes to the suppression of lethal arrhythmias in dnNRSF-Tg mice.

R(−)-Efonidipine, a Highly Selective T-Type Ca^{2+} Channel Blocker, Dramatically Improves Survival Among dnNRSF-Tg Mice

Recently, *R*(−)-efonidipine was shown to be a specific blocker of T-type Ca^{2+} channels.[17,18] To further confirm the

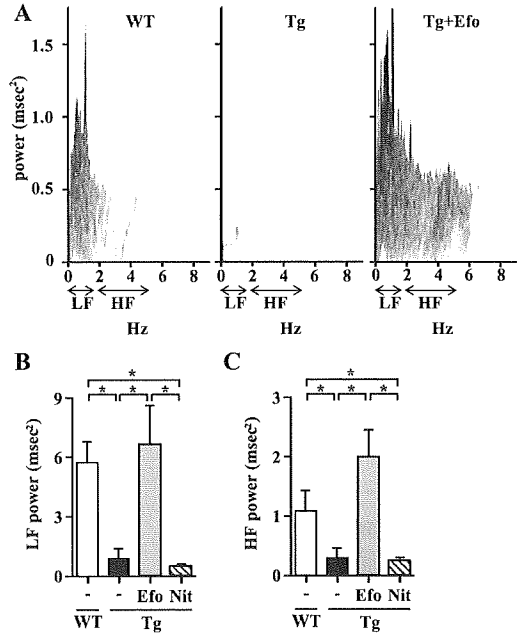

Figure 4. Efonidipine restores cardiac autonomic nervous system function in dnNRSF-Tg mice. A, Representative HRV data from 12-week-old WT and dnNRSF-Tg (Tg) mice treated with or without efonidipine (Efo). Low-frequency (LF) and high-frequency (HF) ranges are shown. B and C, Average power of the LF (B) and HF (C) components of HRV recorded over a 24-hour period in WT and Tg mice treated with or without Efo or nitrendipine (Nit). *$P<0.05$ (n=5 for WT, n=4 for Tg without drugs, n=4 for Tg with Efo, n=4 for Tg with Nit).

beneficial effects of T-type Ca^{2+} channel blockade in the prevention of sudden death in dnNRSF-Tg mice, we administered $R(-)$-efonidipine (200 mg · kg^{-1} · d^{-1} PO) to dnNRSF-Tg mice for 20 weeks. We found that $R(-)$-efonidipine did not significantly affect blood pressure, heart rate, cardiac structure, or systolic function in either WT or dnNRSF-Tg mice compared with vehicle (Figure 6A through 6E). By contrast, $R(-)$-efonidipine dramatically improved the survival rate among dnNRSF-Tg mice, which clearly suggests that T-type Ca^{2+} channel blockade prevents sudden death in dnNRSF-Tg mice (Figure 6F).

Efonidipine Reduces Sudden Death and Arrhythmogenicity in Mice With Acute Myocardial Infarction

Disturbance of cardiac autonomic nervous activity contributes to the incidence of arrhythmogenicity and mortality among patients with chronic heart failure due to nonischemic or ischemic cardiomyopathy, as well as among patients with acute myocardial infarction.[29] To test whether efonidipine can improve the survival rate among mice with a cardiomyopathy other than the nonischemic cardiomyopathy seen in dnNRSF-Tg mice, we administered efonidipine or nitrendipine to WT mice previously subjected to acute myocardial infarction. We found that efonidipine significantly reduced the incidence of sudden death during the subacute phase of myocardial infarction (Figure 7A), although blood pressure, cardiac systolic function, and cardiac structure were all similar in the control, efonidipine, and nitrendipine groups (Figure 7B through 7F). When we further assessed arrhythmogenicity among these mice, we found that control mice with myocardial infarction were highly susceptible to induction of VT and that efonidipine, but not nitrendipine, significantly reduced the frequency of induced VT among mice with myocardial infarction (Figure 7G; online-only Data Supplement Figure II).

Discussion

Ca^{2+} influx is involved in multiple cellular processes, including cell growth, differentiation, and death. In cardiac myocytes, Ca^{2+} influx plays important roles under both normal physiological and pathophysiological conditions. One of the major sources of Ca^{2+} influx in excitable cells is voltage-gated Ca^{2+} channels, which have been classified into several

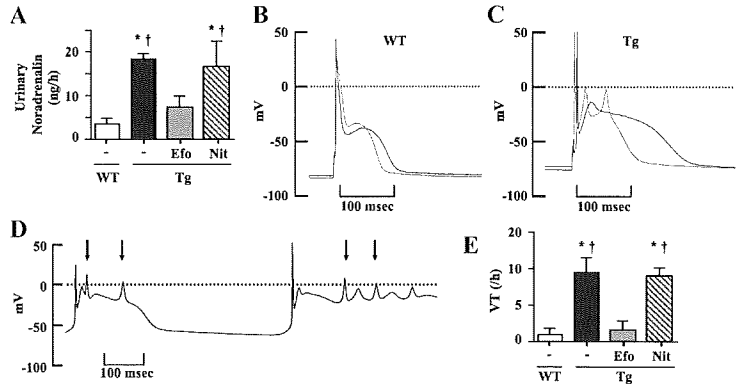

Figure 5. Catecholamine-induced ventricular arrhythmias in dnNRSF-Tg hearts. A, Urinary norepinephrine (noradrenalin) levels in WT and dnNRSF-Tg (Tg) mice treated with or without efonidipine (Efo) or nitrendipine (Nit). *$P<0.05$ vs WT, †$P<0.05$ vs Tg treated with Efo (n=4 for WT, n=6 for Tg without drugs, n=4 for Tg with Efo, n=4 for Tg with Nit). B and C, Representative tracings of action potentials recorded in the presence (red lines) or absence (black lines) of isoproterenol 3 μmol/L from ventricular myocytes isolated from WT (B) and Tg (C) hearts. D, Representative trace showing normal and induced spontaneous action potentials recorded in the presence of isoproterenol 3 μmol/L from ventricular myocytes isolated from Tg hearts. Arrows indicate induced spontaneous action potentials. E, Number of episodes of VT induced in 15 minutes after intraperitoneal administration of isoproterenol (20 μg) to WT or Tg mice treated with or without Efo or Nit. *$P<0.05$ vs WT, †$P<0.05$ vs Tg with Efo. Numbers of mice tested were as follows: WT=5, Tg without drugs=5, Tg with Efo=5, Tg with Nit=4.

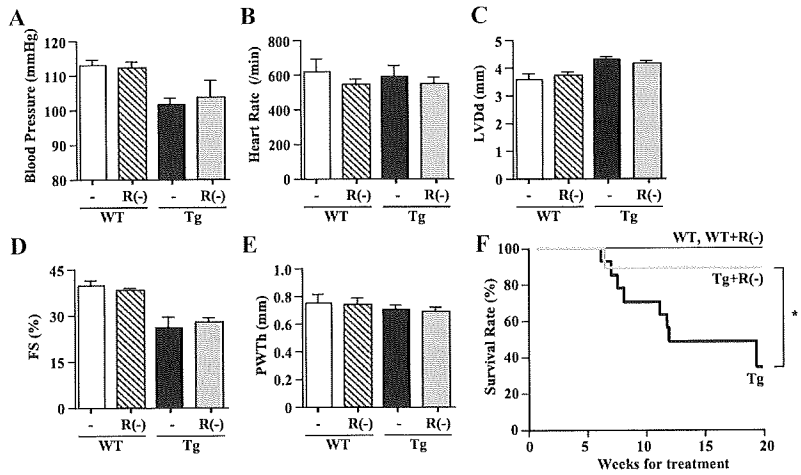

Figure 6. *R*(−)-efonidipine prolongs survival among dnNRSF-Tg mice. A and B, Blood pressures (A) and heart rates (B) in 12-week-old WT and dnNRSF-Tg (Tg) mice treated for 4 weeks with or without *R*(−)-efonidipine [*R*(−)]; n=2 for WT, n=3 for WT with *R*(−), n=5 for Tg, n=4 for Tg with *R*(−). C, D, and E, Left ventricular diastolic dimension (LVDd; C), % fractional shortening (FS; D), and posterior wall thickness (PWTh; E) assessed echocardiographically in 12-week-old WT and Tg mice treated for 4 weeks with or without *R*(−) [n=2 for WT, n=3 for WT with *R*(−), n=4 for Tg and Tg with *R*(−)]. Two-way ANOVA revealed that Tg mice showed decreased blood pressure and enlarged LVDd compared with WT, and *R*(−) had no effect on blood pressure, heart rate, or echocardiographic data. No mice status/medication status interaction was observed [in A, $P<0.001$ between WT and Tg, $P=0.569$ between without and with *R*(−), interaction $P=0.267$; in B, $P<0.725$ between WT and Tg, $P=0.216$ between without and with *R*(−), interaction $P=0.179$; in C, $P<0.001$ between WT and Tg, $P=0.710$ between without and with *R*(−), interaction $P=0.131$; in D, $P<0.001$ between WT and Tg, $P=0.919$ between without and with *R*(−), interaction $P=0.457$; in E, $P=0.304$ between WT and Tg, $P=0.664$ between without and with *R*(−), interaction $P=0.950$]. F, Kaplan-Meier survival curves for WT and Tg mice with or without *R*(−) during a 20-week drug administration period beginning at 8 weeks of age. *$P<0.05$ [n=6 for WT, n=3 for WT with *R*(−), n=13 for Tg, n=9 for Tg with *R*(−)].

types: L (long lasting), T (transient), N (neuronal), P/Q (Purkinje), and R (residual-drug resistant). Generally, cardiac myocytes express only the L and T types.[37] L-type Ca^{2+} channels predominate in mature cardiac myocytes and are crucially involved in excitation-contraction coupling.[37] T-type Ca^{2+} channels are expressed abundantly in embryonic ventricular myocytes.[4,5] After birth, however, expression of T-type Ca^{2+} channels is downregulated in ventricular myocytes,[4,5] so that they are restricted to the conduction system,[3,5] where they modulate pacemaking activities.[3,38] But under conditions of cardiac hypertrophy and heart failure, T-type Ca^{2+} channels are reexpressed in ventricular myocytes,[4,6–8]

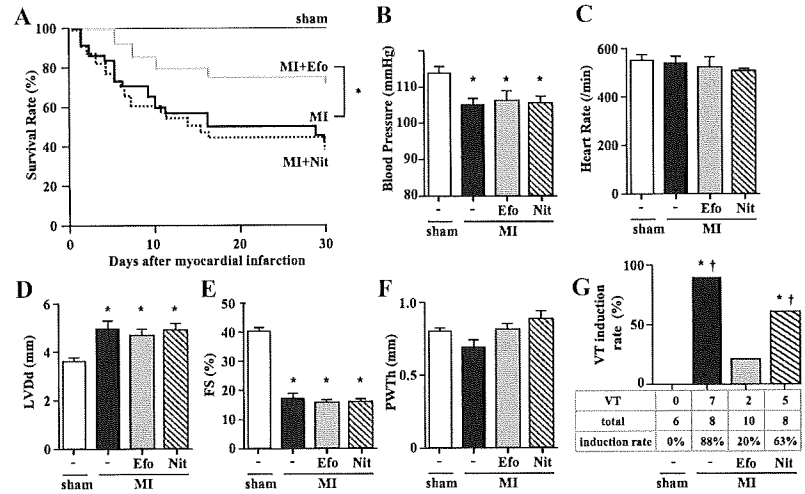

Figure 7. Efonidipine prevented sudden death among mice with acute myocardial infarction. A, Kaplan-Meier survival curves for sham-operated mice (sham) and mice with myocardial infarction (MI) treated for 30 days with or without efonidipine (Efo) or nitrendipine (Nit) beginning at 8 to 12 weeks of age. *$P<0.05$ (n=12 for sham, n=39 for MI, n=29 for MI with Efo, and n=29 for MI with Nit). B and C, Blood pressures (B) and heart rates (C) in sham and MI mice treated for 4 weeks with or without Efo or Nit. *$P<0.05$ vs sham (n=7 in each group). D, E, and F, Left ventricular diastolic dimension (LVDd; D), % fractional shortening (FS; E), and posterior wall thickness (PWTh; F) assessed echocardiographically in sham and MI mice treated for 4 weeks with or without Efo or Nit. *$P<0.05$ vs sham (n=10 for sham, n=6 for MI, n=10 for MI with Efo, and n=8 for MI with Nit). G, Frequency of mice with inducible VT in sham and MI mice treated for 4 weeks with or without Efo or Nit are shown. VT indicates number of mice with inducible VT; total, total number of mice tested. *$P<0.05$ vs WT, †$P<0.05$ vs MI with Efo.

and they are thought to be involved in the altered cardiac function and arrhythmogenicity seen in the diseased myocardium.[2,3] Consistent with that idea, the dual T- and L-type Ca^{2+} channel blocker mibefradil attenuates the pathological processes seen in some animal models of cardiac disease.[10,11,39] Moreover, it was recently reported that genetic deletion of *CACNA1H* results in resistance to pathological cardiac hypertrophy.[9] Nonetheless, the effect of T-type Ca^{2+} channel blockade on the incidence of malignant arrhythmias and sudden death remains unknown.

In the present study, we demonstrated that the dual T- and L-type Ca^{2+} channel blocker efonidipine prevents the sudden death and arrhythmogenicity otherwise seen in dnNRSF-Tg mice, whereas nitrendipine, a selective L-type Ca^{2+} channel blocker, does not. Suppression of arrhythmogenicity also was observed when dnNRSF-Tg mice were treated with mibefradil. Although the doses of nitrendipine used in the present studies (20 and 60 mg/kg) did not significantly affect blood pressure in dnNRSF-Tg mice, those doses previously were shown to effectively block L-type Ca^{2+} channels in mice.[19] We also observed that treatment of db/db mice, a mouse model of type 2 diabetes–associated hypertension,[40] with nitrendipine 10 mg $\cdot$ kg^{-1} $\cdot$ d^{-1} for 8 days significantly reduced their elevated blood pressure (unpublished observation). These results clearly demonstrate that blockade of T-type Ca^{2+} channels, not L-type Ca^{2+} channels, mediates the effects of efonidipine and mibefradil on dnNRSF-Tg mice, although there is still the possibility that unknown effects of efonidipine and mibefradil on other currents are responsible. Furthermore, *R*(−)-efonidipine, a recently identified specific blocker of T-type Ca^{2+} channels,[17,18] dramatically improved the survival rate among dnNRSF-Tg mice, which strongly supports the notion that T-type Ca^{2+} channels play a key role in mediating the lethal arrhythmias seen in this animal model. In addition, efonidipine, but not nitrendipine, also reduced the incidence of sudden death and arrhythmias among mice with acute myocardial infarction. Collectively, the lines of evidence summarized above demonstrate that T-type Ca^{2+} channel blockade prevents sudden death and malignant arrhythmias in mice with heart failure caused by either nonischemic or ischemic myocardial injury.

Abnormalities in atrial and ventricular electrophysiology are well-recognized contributors to arrhythmogenesis in diseased human hearts.[1] In dnNRSF-Tg mice, the action potential is prolonged, and the resting membrane potential is depolarized, which is consistent with features observed in failing human hearts.[1] Notably, efonidipine significantly restored the resting membrane potential in ventricular myocytes from dnNRSF-Tg mice. Given that membrane depolarization can enhance arrhythmogenicity by inducing triggered activity mediated by early afterdepolarizations or delayed afterdepolarizations and by increasing automaticity,[1] restoration of the resting membrane potential is likely 1 of the mechanisms by which efonidipine prevents ventricular arrhythmias and sudden cardiac death in dnNRSF-Tg mice. Although we still do not fully understand the mechanism by which T-type Ca^{2+} channel blockade restores the membrane potential in dnNRSF-Tg cardiomyocytes, the activation and availability of $I_{Ca,T}$ overlap at membrane potentials in the range of −60 to −30 mV, which could contribute to a pathological Ca^{2+} leak into cells during diastole.[3] It was recently reported that elevation of diastolic Ca^{2+} reduced the amplitude of I_{K1}, which is a critical determinant of resting membrane potential in ventricular myocytes.[41] In fact, the amplitude of I_{K1} was reduced significantly in dnNRSF-Tg ventricular myocytes (unpublished observation). It was also recently shown with mice lacking *CACNA1H* that the α1H T-type Ca^{2+} channel plays a pivotal role in the induction of pathological calcineurin/nuclear factor–activated T cell signaling, which increases susceptibility to arrhythmias.[9,42,43] T-type Ca^{2+} channel blockade may correct abnormalities in ventricular electrophysiology in part by inhibiting these pathological signaling pathways.

Disturbance of cardiac autonomic nervous activity that leads to increased sympathetic nerve activity and decreased parasympathetic nerve activity contributes to the increased arrhythmogenicity seen in patients with chronic heart failure.[44] HRV analysis is widely used to assess autonomic nerve function in the heart and has been shown to correlate with the prognosis of patients with heart failure.[31,32] In the present study, efonidipine clearly reversed the altered HRV seen in dnNRSF-Tg mice. L-type Ca^{2+} channel blockers generally enhance sympathetic nerve activity and reduce parasympathetic nerve activity.[34,45] By contrast, efonidipine appears to have the opposite effects on autonomic nerve activity. In a previous study performed in mildly to moderately hypertensive patients, mibefradil enhanced parasympathetic nervous activity.[34] Similarly, in another study of hypertensive patients, efonidipine improved the disturbed balance in autonomic nerve activity in the heart.[35] The involvement of T-type Ca^{2+} channels in the release of neurotransmitters, including catecholamines, from neuronal and endocrine cells may account for the effects of T-type Ca^{2+} channel blockade on autonomic nerve activity.[33] Consistent with that idea, we observed in the present study that efonidipine significantly reduces the increase in urinary norepinephrine excretion otherwise seen in dnNRSF-Tg mice. Thus, along with its direct effects on the electrophysiology of ventricular myocytes, the effects of efonidipine on cardiac autonomic function likely contribute to the prevention of malignant arrhythmias and sudden death in dnNRSF-Tg mice. There is also the possibility that correcting the balance between sympathetic and parasympathetic nerve activity affects the electrophysiological properties of ventricular myocytes. The present results showing that efonidipine reduces the incidence of sudden death among mice with acute myocardial infarction further support the idea that correcting the balance in cardiac autonomic nerve activity through blockade of T-type Ca^{2+} channels contributes to the prevention of malignant arrhythmias and sudden death by efonidipine, because disturbances in cardiac autonomic nervous activity are associated with sudden death in patients with acute myocardial infarction.[46,47]

Mibefradil was approved for use in the treatment of hypertension, angina pectoris, and congestive heart failure in 1997 but was withdrawn from the market because of an unexpected side effect unrelated to the T-type Ca^{2+} channel blockade: It inhibited cytochrome p450s, thereby causing negative drug-drug interactions.[2] On the other hand, efonidip-

ine has been used to treat hypertension for several years in Japan, and no such severe side effects have yet been identified. Although further investigation is necessary, we suggest that efonidipine or some other T-type Ca^{2+} channel blockers, including the *R*(−)-isomer efonidipine, may be clinically useful for the prevention of sudden arrhythmic death in patients with heart failure.

Acknowledgments

We thank Yukari Kubo for her excellent secretarial work.

Sources of Funding

This research was supported by a grant-in-aid for scientific research from the Japan Society for the Promotion of Science (to Dr Kuwahara., Dr Harada, and Dr Nakao.), and grants from the Japanese Ministry of Health, Labor and Welfare (to Dr Nakao) and from the Japan Heart Foundation/Pfizer Pharmaceuticals Inc Grant on Cardiovascular Disease Research, the Japan Heart Foundation/ Novartis Grant for Research Award on Molecular and Cellular Cardiology, the Mochida Memorial Foundation for Medical and Pharmaceutical Research, the Uehara Memorial Foundation, the Ichiro Kanehara Foundation, the Astellas Foundation for Research on Metabolic Disorders, the Mitsubishi Foundation, the Suzuken Memorial Foundation, the Takeda Medical Research Foundation, and the Kanae Foundation for the Promotion of Medical Science (to Dr Kuwahara).

Disclosures

None.

References

1. Tomaselli GF, Marbán E. Electrophysiological remodeling in hypertrophy and heart failure. *Cardiovasc Res.* 1999;42:270–283.
2. Clozel JP, Ertel EA, Ertel SI. Voltage-gated T-type Ca^{2+} channels and heart failure. *Proc Assoc Am Physicians.* 1999;111:429–437.
3. Vassort G, Talavera K, Alvarez JL. Role of T-type Ca^{2+} channels in the heart. *Cell Calcium.* 2006;40:205–220.
4. Yasui K, Niwa N, Takemura H, Opthof T, Muto T, Horiba M, Shimizu A, Lee JK, Honjo H, Kamiya K, Kodama I. Pathophysiological significance of T-type Ca^{2+} channels: expression of T-type Ca^{2+} channels in fetal and diseased heart. *J Pharmacol Sci.* 2005;99:205–210.
5. Niwa N, Yasui K, Opthof T, Takemura H, Shimizu A, Horiba M, Lee JK, Honjo H, Kamiya K, Kodama I. Cav3.2 subunit underlies the functional T-type Ca^{2+} channel in murine hearts during the embryonic period. *Am J Physiol Heart Circ Physiol.* 2004;286:H2257–H2263.
6. Nuss HB, Houser SR. T-type Ca^{2+} current is expressed in hypertrophied adult feline left ventricular myocytes. *Circ Res.* 1993;73:777–782.
7. Sen L, Smith TW. T-type Ca^{2+} channels are abnormal in genetically determined cardiomyopathic hamster hearts. *Circ Res.* 1994;75:149–155.
8. Martinez ML, Heredia MP, Delgado C. Expression of T-type Ca(2+) channels in ventricular cells from hypertrophied rat hearts. *J Mol Cell Cardiol.* 1999;31:1617–1625.
9. Chiang CS, Huang CH, Chieng H, Chang YT, Chang D, Chen JJ, Chen YC, Chen YH, Shin HS, Campbell KP, Chen CC. The Ca (v) 3.2 T-type Ca(2+) channel is required for pressure overload-induced cardiac hypertrophy in mice. *Circ Res.* 2009;104:522–530.
10. Villame J, Massicotte J, Jasmin G, Dumont L. Effects of mibefradil, a T- and L-type calcium channel blocker, on cardiac remodeling in the UM-X7.1 cardiomyopathic hamster. *Cardiovasc Drugs Ther.* 2001;15: 41–48.
11. Sandmann S, Min JY, Meissner A, Unger T. Effects of the calcium channel antagonist mibefradil on haemodynamic parameters and myocardial Ca(2+)-handling in infarct-induced heart failure in rats. *Cardiovasc Res.* 1999;44:67–80.
12. Mulder P, Richard V, Compagnon P, Henry JP, Lallemand F, Clozel JP, Koen R, Mace B, Thuillez C. Increased survival after long-term treatment with mibefradil, a selective T-channel calcium antagonist, in heart failure. *J Am Coll Cardiol.* 1997;29:416–421.
13. Kuwahara K, Saito Y, Ogawa E, Takahashi N, Nakagawa Y, Naruse Y, Harada M, Hamanaka I, Izumi T, Miyamoto Y, Kishimoto I, Kawakami R, Nakanishi M, Mori N, Nakao K. The neuron-restrictive silencer element-neuron-restrictive silencer factor system regulates basal and endothelin 1-inducible atrial natriuretic peptide gene expression in ventricular myocytes. *Mol Cell Biol.* 2001;21:2085–2097.
14. Kuwahara K, Saito Y, Takano M, Arai Y, Yasuno S, Nakagawa Y, Takahashi N, Adachi Y, Takemura G, Horie M, Miyamoto Y, Morisaki T, Kuratomi S, Noma A, Fujiwara H, Yoshimasa Y, Kinoshita H, Kawakami R, Kishimoto I, Nakanishi M, Usami S, Saito Y, Harada M, Nakao K. NRSF regulates the fetal cardiac gene program and maintains normal cardiac structure and function. *EMBO J.* 2003;22:6310–6321.
15. Masumiya H, Shijuku T, Tanaka H, Shigenobu K. Inhibition of myocardial L- and T-type Ca^{2+} currents by efonidipine: possible mechanism for its chronotropic effect. *Eur J Pharmacol.* 1998;349:351–357.
16. Horiba M, Muto T, Ueda N, Opthof T, Miwa K, Hojo M, Lee JK, Kamiya K, Kodama I, Yasui K. T-type Ca^{2+} channel blockers prevent cardiac cell hypertrophy through an inhibition of calcineurin-NFAT3 activation as well as L-type Ca^{2+} channel blockers. *Life Sci.* 2008:82:554–560.
17. Tanaka H, Komikado C, Shimada H, Takeda K, Namekata I, Kawanishi T, Shigenobu K. The R(-)-enantiomer of efonidipine blocks T-type but not L-type calcium current in guinea pig ventricular myocardium. *J Pharmacol Sci.* 2004;96:499–501.
18. Furukawa T, Miura R, Honda M, Kamiya N, Mori Y, Takeshita S, Isshiki T, Nukada T. Identification of R(-)-isomer of efonidipine as a selective blocker of T-type Ca^{2+} channels. *Br J Pharmacol.* 2004;143:1050–1057.
19. Jinnah HA, Yitta S, Drew T, Kim BS, Visser JE, Rothstein JD. Calcium channel activation and self-biting in mice. *Proc Natl Acad Sci U S A.* 1999;96:15228–15232.
20. Shudo C, Masuda Y, Sugita H, Tamura T, Furukawa S, Hayashi K, Hirata H, Shikada K, Tanaka S, Tomita K. Effects of efonidipine, nicardipine and captopril on proteinuria in aged spontaneously hypertensive rats. *Arzneimittelforschung.* 1996;46:852–854.
21. Furukawa T, Nukada T, Miura R, Ooga K, Honda M, Watanabe S, Koganesawa S, Isshiki T. Differential blocking action of dihydropyridine Ca^{2+} antagonists on a T-type Ca^{2+} channel (alpha1G) expressed in Xenopus oocytes. *J Cardiovasc Pharmacol.* 2005;45:241–246.
22. Yokoyama U, Minamisawa S, Adachi-Akahane S, Akaike T, Naguro I, Funakoshi K, Iwamoto M, Nakagome M, Uemura N, Hori H, Yokota S, Ishikawa Y. Multiple transcripts of Ca^{2+} channel alpha1-subunits and a novel spliced variant of the alpha1C-subunit in rat ductus arteriosus. *Am J Physiol Heart Circ Physiol.* 2006;290:H1660–H1670.
23. Kawakami R, Saito Y, Kishimoto I, Harada M, Kuwahara K, Takahashi N, Nakagawa Y, Nakanishi M, Tanimoto K, Usami S, Yasuno S, Kinoshita H, Chusho H, Tamura N, Ogawa Y, Nakao K. Overexpression of brain natriuretic peptide facilitates neutrophil infiltration and cardiac matrix metalloproteinase-9 expression after acute myocardial infarction. *Circulation.* 2004;110:3306–3312.
24. Shioya T. A simple technique for isolating healthy heart cells from mouse models. *J Physiol Sci.* 2007;57:327–335.
25. Gehrmann J, Berul CI. Cardiac electrophysiology in genetically engineered mice. *J Cardiovasc Electrophysiol.* 2000;11:354–368.
26. Mukoyama M, Nakao K, Hosoda K, Suga S, Saito Y, Ogawa Y, Shirakami G, Jougasaki M, Obata K, Yasue H. Brain natriuretic peptide as a novel cardiac hormone in humans: evidence for an exquisite dual natriuretic peptide system, atrial natriuretic peptide and brain natriuretic peptide. *J Clin Invest.* 1991;87:1402–1412.
27. Nakagawa O, Ogawa Y, Itoh H, Suga S, Komatsu Y, Kishimoto I, Nishino K, Yoshimasa T, Nakao K. Rapid transcriptional activation and early mRNA turnover of brain natriuretic peptide in cardiocyte hypertrophy: evidence for brain natriuretic peptide as an "emergency" cardiac hormone against ventricular overload. *J Clin Invest.* 1995;96:1280–1287.
28. Leuranguer V, Mangoni ME, Nargeot J, Richard S. Inhibition of T-type and L-type calcium channels by mibefradil: physiologic and pharmacologic bases of cardiovascular effects. *J Cardiovasc Pharmacol.* 2001; 37:649–661.
29. Task Force of the European Society of Cardiology and the North American Society of Pacing and Electrophysiology. Heart rate variability: standards of measurement, physiological interpretation and clinical use. *Circulation.*1996;93:1043–1065.
30. Guzzetti S, Cogliati C, Turiel M, Crema C, Lombardi F, Malliani A. Sympathetic predominance followed by functional denervation in the progression of chronic heart failure. *Eur Heart J.* 1995;16:1100–1107.
31. La Rovere MT, Pinna GD, Maestri R, Mortara A, Capomolla S, Febo O, Ferrari R, Franchini M, Gnemmi M, Opasich C, Riccardi PG, Traversi E, Cobelli F. Short-term heart rate variability strongly predicts sudden

cardiac death in chronic heart failure patients. *Circulation*. 2003;107:565–570.
32. Sandercock GR, Brodie DA. The role of heart rate variability in prognosis for different modes of death in chronic heart failure. *Pacing Clin Electrophysiol*. 2006;29:892–904.
33. Carbone E, Giancippoli A, Marcantoni A, Guido D, Carabelli V. A new role for T-type channels in fast "low-threshold" exocytosis. *Cell Calcium*. 2006;40:147–154.
34. Pellizzer AM, Kamen PW, Esler MD, Lim S, Krum H. Comparative effects of mibefradil and nifedipine gastrointestinal transport system on autonomic function in patients with mild to moderate essential hypertension. *J Hypertens*. 2001;19:279–285.
35. Harada K, Nomura M, Nishikado A, Uehara K, Nakaya Y, Ito S. Clinical efficacy of efonidipine hydrochloride, a T-type calcium channel inhibitor, on sympathetic activities. *Circ J*. 2003;67:139–145.
36. Just A, Faulhaber J, Ehmke H. Autonomic cardiovascular control in conscious mice. *Am J Physiol Regul Integr Comp Physiol*. 2000;279:R2214–R2221.
37. Bers DM. Cardiac excitation-contraction coupling. *Nature*. 2002;415:198–205.
38. Huser J, Blatter LA, Lipsius SL. Intracellular Ca^{2+} release contributes to automaticity in cat atrial pacemaker cells. *J Physiol*. 2000;524(part 2):415–422.
39. Sandmann S, Bohle RM, Dreyer T, Unger T. The T-type calcium channel blocker mibefradil reduced interstitial and perivascular fibrosis and improved hemodynamic parameters in myocardial infarction-induced cardiac failure in rats. *Virchows Arch*. 2000;436:147–157.
40. Su W, Guo Z, Randall DC, Cassis L, Brown DR, Gong MC. Hypertension and disrupted blood pressure circadian rhythm in type 2 diabetic db/db mice. *Am J Physiol Heart Circ Physiol*. 2008;295:H1634–H1641.
41. Fauconnier J, Lacampagne A, Rauzier JM, Vassort G, Richard S. Ca^{2+}-dependent reduction of I_{K1} in rat ventricular cells: a novel paradigm for arrhythmia in heart failure? *Cardiovasc Res*. 2005;68:204–212.
42. Dong D, Duan Y, Guo J, Roach DE, Swirp SL, Wang L, Lees-Miller JP, Sheldon RS, Molkentin JD, Duff HJ. Overexpression of calcineurin in mouse causes sudden cardiac death associated with decreased density of K+ channels. *Cardiovasc Res*. 2003;57:320–332.
43. Khoo MS, Li J, Singh MV, Yang Y, Kannankeril P, Wu Y, Grueter CE, Guan X, Oddis CV, Zhang R, Mendes L, Ni G, Madu EC, Yang J, Bass M, Gomez RJ, Wadzinski BE, Olson EN, Colbran RJ, Anderson ME. Death, cardiac dysfunction, and arrhythmias are increased by calmodulin kinase II in calcineurin cardiomyopathy. *Circulation*. 2006;114:1352–1359.
44. Anderson KP. Sympathetic nervous system activity and ventricular tachyarrhythmias: recent advances. *Ann Noninvasive Electrocardiol*. 2003;8:75–89.
45. Minami J, Ishimitsu T, Kawano Y, Matsuoka H. Effects of amlodipine and nifedipine retard on autonomic nerve activity in hypertensive patients. *Clin Exp Pharmacol Physiol*. 1998;25:572–576.
46. Ewing DJ. Heart rate variability: an important new risk factor in patients following myocardial infarction. *Clin Cardiol*. 1991;14:683–685.
47. Weiss JN, Nademanee K, Stevenson WG, Singh B. Ventricular arrhythmias in ischemic heart disease. *Ann Intern Med*. 1991;114:784–797.

CLINICAL PERSPECTIVE

Despite recent progress in nonpharmacological therapy, pharmacological interventions for the treatment and prevention of lethal arrhythmias associated with heart failure remain limited. In this study, we used mouse models of ischemic and nonischemic cardiomyopathy to show that T-type Ca^{2+} channel blockade diminishes arrhythmogenicity and prevents sudden death in heart failure. The dual T- and L-type Ca^{2+} channel blocker mibefradil was withdrawn from the market because of an unexpected side effect unrelated to the T-type Ca^{2+} channel blockade: It inhibited cytochrome p450s, thereby causing negative drug-drug interactions. Another dual T- and L-type Ca^{2+} channel blocker, efonidipine, which we used in this study, has been used in Japan for several years to treat hypertension, and no severe side effects have yet been identified. Although further investigation is necessary, our results suggest that efonidipine and perhaps other T-type Ca^{2+} channel blockers, especially selective T-type Ca^{2+} channel blockers such as the *R*(−)-isomer efonidipine, may be clinically useful for the prevention of lethal arrhythmias and sudden death in patients with heart failure.

FEBS Letters 583 (2009) 2067–2070

ELSEVIER

FEBS Letters

journal homepage: www.FEBSLetters.org

Inhibition of hepatic damage and liver fibrosis by brain natriuretic peptide

Takuhiro Sonoyama, Naohisa Tamura *, Kazutoshi Miyashita, Kwijun Park, Naofumi Oyamada, Daisuke Taura, Megumi Inuzuka, Yasutomo Fukunaga, Masakatsu Sone, Kazuwa Nakao

Department of Medicine and Clinical Science, Kyoto University Graduate School of Medicine, 54 Shogoin-Kawahara-cho, Sakyo-ku, Kyoto 606-8507, Japan

ARTICLE INFO

Article history:
Received 15 January 2009
Revised 11 May 2009
Accepted 14 May 2009
Available online 20 May 2009

Edited by Veli-Pekka Lehto

Keywords:
Brain natriuretic peptide
Guanylyl cyclase-A
Carbon tetrachloride
Liver fibrosis
Hepatic stellate cell

ABSTRACT

Anti-fibrotic and organ protective effects of brain natriuretic peptide (BNP) have been reported. In this study, effects of BNP on liver fibrosis were examined in the carbon tetrachloride (CCl_4)-induced liver fibrosis model using BNP-transgenic (Tg) and wild-type (WT) mice. Twice-a-week intraperitoneal injections of CCl_4 for 8 weeks resulted in massive liver fibrosis, augmented transforming growth factor (TGF)-β_1 and type I procollagen α_1 chain (Col1a1) mRNA expression, and the hepatic stellate cell (HSC) activation in WT mice, all of which were significantly suppressed in Tg mice. These observations indicate that BNP inhibits liver fibrosis by attenuating the activation of HSCs.

1. Introduction

Natriuretic peptides (NPs) are a family of peptides, which consist of atrial, brain, and C-type NPs (ANP, BNP, and CNP, respectively) [1]. NPs' biological actions are mainly mediated by two NP receptors: guanylyl cyclase (GC)-A and GC-B [1]. NPs increase intracellular cGMP concentrations upon ligand binding. ANP and BNP are cardiac hormones produced mainly in the cardiac atria and ventricles, respectively, and play important roles to maintain cardiovascular homeostasis by activating GC-A [1]. CNP binds to GC-B, and the CNP/GC-B system takes part in the endochondral ossification and the vascular remodeling [1].

Carbon tetrachloride (CCl_4)-induced liver fibrosis is one of the most utilized animal models for liver fibrosis. CCl_4 selectively damage hepatocytes around central veins (centrilobular regions), which highly express cytochrome P450 2E1 (CYP2E1) that change CCl_4 into reactive oxygen species (ROS) [2]. Damaged hepatocytes recruit leukocytes and stimulate Kupffer cells to secrete several proinflammatory cytokines such as tumor necrosis factor-α, which activate hepatic stellate cells (HSCs). Transforming growth factor (TGF)-β_1 released from damaged hepatocytes also activates adjacent HSCs [3]. Activated HSCs become myofibroblast-like cells, which express α-smooth muscle actin (SMA), intensely proliferate, profoundly synthesize collagen, and produce profibrotic cytokines including TGF-β_1, leading to the development of liver fibrosis [3]. Also in non-alcoholic steatohepatitis (NASH) and alcoholic steatohepatitis, CYP2E1-derived ROS induce hepatocellular damage and HSC activation, leading to liver fibrosis [2,4].

While antifibrotic effects of CNP were shown in lungs and hearts of experimental animal models [5,6], we showed antifibrotic effects of BNP in the heart and kidneys [7,8]. In this study, we used BNP-transgenic (Tg) mice [9] in the CCl_4-induced liver fibrosis model to investigate effects of BNP on liver damage and fibrosis.

2. Materials and methods

2.1. Animals

Male wild-type (WT) C57BL/6J mice (Shimizu Experimental Supplies, Kyoto, Japan) and male BNP-Tg mice of line 75 overexpressing BNP (8 weeks of age, 25–30 g of body weight) were used. The BNP-Tg mice harbor a transgene that expresses BNP under the control of the human serum amyloid P promoter, which is active in the liver after birth, and their plasma BNP concentrations were comparable to those in patients with severe congestive

Abbreviations: BNP, brain natriuretic peptide; CCl_4, carbon tetrachloride; Tg, transgenic; WT, wild-type; TGF, transforming growth factor; Col1a1, type I procollagen α_1 chain; HSC(s), hepatic stellate cell(s) NP, natriuretic peptide; ANP, atrial natriuretic peptide; CNP, C-type natriuretic peptide; GC, guanylyl cyclase; ROS, reactive oxygen species; CYP2E1, cytochrome P450 2E1; NASH, non-alcoholic steatohepatitis; SMA, smooth muscle actin; DMN, dimethylnitrosamine

* Corresponding author. Fax: +81 75 771 9452.
E-mail address: ntamura@kuhp.kyoto-u.ac.jp (N. Tamura).

0014-5793/$36.00
doi:10.1016/j.febslet.2009.05.025

heart failure [9]. Concentrations of BNP-like immunoreactivities in their livers were about 10-fold higher than their plasma BNP concentrations, but the majority of BNP-like immunoreactivities in their livers were proBNP, which is less active than mature peptide [9]. Mice were housed in a specified pathogen free facility with a 12-h light/dark cycle. Access to food and water was *ad libitum* throughout the study period. Mice were intraperitoneally injected with CCl_4 of 1 ml/kg body weight twice a week for 2–8 weeks to induce liver fibrosis. Mice were killed with the intraperitoneal injection of pentobarbital 3 days after the final CCl_4 injection, and livers were either fixed with 4% phosphate-buffered paraformaldehyde and embedded in paraffin for histological examination or immediately frozen in liquid nitrogen for the extraction of RNA. The experimental protocol of this study is approved by the Animal Research Committee, Kyoto University.

2.2. Histological analyses

Tissue sections were stained with hematoxylin and eosin or Sirius red to evaluate histological changes and collagen fiber deposition, respectively. To quantify the extent of fibrosis, percentages of Sirius red-positive pixels were measured in five randomly selected microscope fields at 40× magnification and averaged for each specimen by a technician, who did not know the genotype of each specimen. The sections were also subjected to immunohistochemistry with an antibody against mouse α-SMA (M0851, DAKO, Denmark), as described previously [10].

2.3. Extraction and analysis of RNA

Total RNA extracted from livers using an RNeasy Mini kit (Qiagen, Tokyo, Japan) was reverse-transcribed using a PrimeScript RT-PCR kit (Takara Bio, Otsu, Japan), and subjected to a real-time quantitative PCR using an ABI Prism 7300 Sequence Detection System (Applied Biosystems, Foster City, CA) with SYBR Premix Ex Taq (Takara Bio, Otsu, Japan) to evaluate mRNA levels of TGF-β_1, type I procollagen α1 chain (Col1a1), and α-SMA, according to the manufacturers' instructions. Levels of mRNA were normalized with those of a house keeping gene, β-actin. The primers used are shown in Supplementary Table 1.

2.4. Statistics

All values are expressed as means ± standard errors of the mean. Statistical differences in averages between two groups and among three or more groups were assessed by unpaired *t*-test and ANOVA, respectively.

3. Results and discussion

Before CCl_4 injections and after 2 weeks of repeated CCl_4 injections, hepatocellular damage and liver fibrosis were not evident both in WT and Tg mice (Fig. 1A and B). In WT mice, hepatocellular necrosis with inflammatory cell infiltration and fibrosis appeared in centrilobular regions after 4 weeks of CCl_4 injections (Fig. 1C), and hepatocellular necrosis was observed throughout the liver and septal fibrosis emerging from centrilobular regions formed central–central bridging necrosis after 8 weeks of CCl_4 injections (Fig. 1D). This is the typical time course of histological changes in this model [3], showing the model was adequately prepared in this study. In Tg mice, the extent of liver fibrosis was significantly suppressed compared with that of WT mice after 8 weeks of CCl_4 injections (Fig. 1D and E).

Hepatic TGF-β_1 and Col1a1 mRNA levels were not different between WT and Tg mice before CCl_4 injections (Fig. 2). After 2 weeks of CCl_4 injections, hepatic TGF-β_1 and Col1a1 mRNA levels tended to increase compared with those before CCl_4 injections in WT mice,

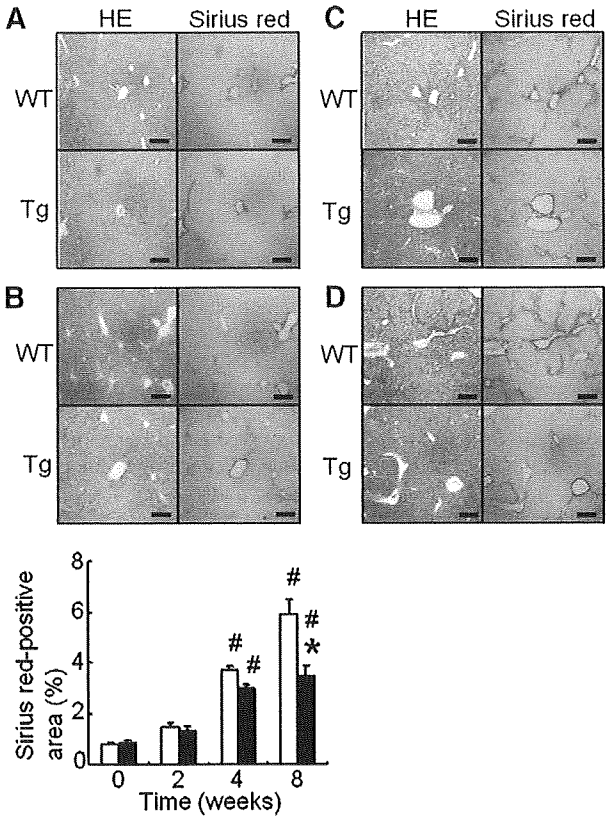

Fig. 1. Typical images of Hematoxylin and Eosin (HE) and Sirius red staining of livers from wild-type (WT) and BNP-transgenic (Tg) mice before CCl_4 injections (A), and after 2 (B), 4 (C), and 8 weeks of twice-a-week CCl_4 injections (D) are shown. Scale bars indicate 100 μm. Collagen fibrils are stained red by Sirius red. (E) The extent of liver fibrosis is quantified as the percentage of Sirius red-positive areas (before CCl_4 injections, $n = 5$ for each genotype; after 2, 4, and 8 weeks of CCl_4 injections, $n = 4$, 4, and 8 for each genotype, respectively). Data of WT and Tg mice are shown with open and closed columns, respectively. $^*P < 0.05$ vs. WT mice at each time point; $^\#P < 0.05$ vs. before CCl_4 injections in the same genotype by ANOVA.

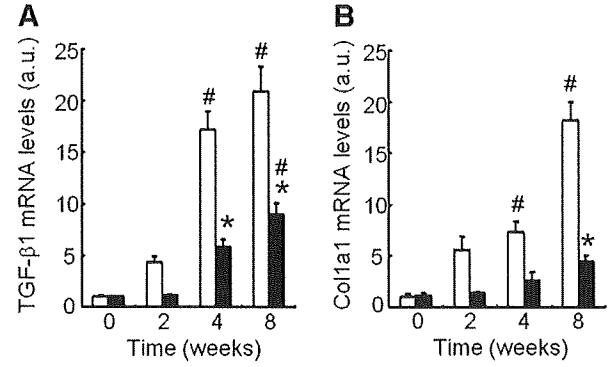

Fig. 2. Real-time quantitative PCR analysis of hepatic transforming growth factor (TGF)-β_1 (A) and type I procollagen α_1 chain (Col1a1) (B) mRNA levels in wild-type (WT, open columns) and BNP-transgenic (Tg, closed columns) mice before CCl_4 injections ($n = 5$ for each genotype) and after 2, 4, and 8 weeks of CCl_4 injections ($n = 4$, 4, and 8 for each genotype, respectively). The average of mRNA levels of each gene in WT livers before CCl_4 injections is set 1.0 arbitrary unit (a.u.). $^*P < 0.05$ vs. WT mice at each time point; $^\#P < 0.05$ vs. before CCl_4 injections in the same genotype by ANOVA.

while they remained similar to those before CCl_4 injections in Tg mice (Fig. 2). After 4 or 8 weeks of CCl_4 injections, hepatic TGF-β_1 and Col1a1 mRNA levels significantly increased compared with those before CCl_4 injections in WT mice (Fig. 2). Only TGF-β_1 mRNA levels were suppressed in Tg mice compared with those in WT mice after 4 weeks of CCl_4 injections, and both TGF-β_1 and Col1a1 mRNA levels were suppressed in Tg mice compared with those in WT mice after 8 weeks of CCl_4 injections (Fig. 2). We reported that BNP suppresses TGF-β_1 and Col1a1 mRNA levels and exerts anti-fibrotic and organ protective effects in the heart and kidneys [7,8]. This study added the liver to targets of those effects of BNP.

Alpha-SMA-positive cells, which are activated, myofibroblastic HSCs, were not detected in livers of WT and Tg mice before CCl_4 injections (Fig. 3A). After 8 weeks of CCl_4 injections, lots of α-SMA-positive cells were observed in regions of bridging necrosis in WT mice, but they were hardly seen in Tg mice (Fig. 1D and 3A). Hepatic α-SMA mRNA levels were attenuated in Tg mice compared with WT mice after 8 weeks of CCl_4 injections (Fig. 3B).

An *in vitro* study showed that activated human HSCs expressed GC-B without GC-A, suggesting that CNP has a potential to prevent HSCs' activation via GC-B and to counteract liver fibrosis [11]. On the contrary, it was reported that both quiescent and activated human HSCs expressed GC-A mRNA [13]. It was also reported that HSCs isolated from rats with CCl_4-induced cirrhosis expressed a higher number of ANP receptors compared with HSCs isolated from normal rats, indicating that *in vivo* activation of HSCs is associated with an up-regulation of ANP receptors [12]. GC-A mRNA expression was detected also in hepatocytes and Kupffer cells isolated from rat livers, and ANP could prevent ischemia-reperfusion injury of rat livers, which was caused by ROS generated by Kupffer cells, via GC-A [13]. During the course of our experiments, Ishigaki and colleagues reported that a continuously intravenous infusion of ANP could suppress dimethylnitrosamine (DMN)-induced liver damage and fibrosis by inhibiting HSC activation in rats [14]. It is speculated that an activation of GC-A can prevent liver fibrosis due to hepatocellular damage, because either an intravenous administration of ANP in rats or increased circulating BNP concentrations in Tg mice could prevent hepatocellular damage and liver fibrosis in different experimental models.

In the heart, signaling through GC-A inhibits angiotensin II type I receptor-mediated cardiac hypertrophy and fibrosis [15]. Olmesartan, an angiotensin II receptor blocker, reportedly inhibited liver fibrosis caused by NASH in mice [16]. An activation of GC-A might inhibit the renin–angiotensin system to protect the liver, but further studies will be needed to clarify the precise molecular mechanisms.

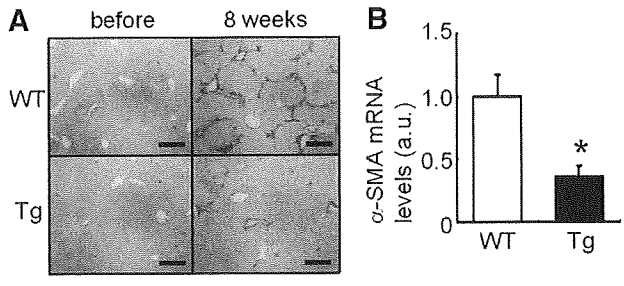

Fig. 3. Hapatic stellate cell activation in carbon tetrachloride-induced liver fibrosis. (A) Immunohistochemical detections of α-smooth muscle actin (SMA) in livers of wild-type (WT) and BNP-transgenic (Tg) mice before and after 8 weeks of CCl_4 injections. Scale bars indicate 100 μm. (B) Real-time quantitative PCR analysis of hepatic α-SMA mRNA levels in WT and Tg mice after 8 weeks of CCl_4 injections ($n = 8$ for each genotype). The average of mRNA levels in WT livers is set 1.0 arbitrary unit (a.u.). $^*P < 0.05$ vs. WT mice by unpaired *t*-test.

In conclusion, BNP could inhibit the CCl_4-induced liver fibrosis through the prevention of hepatocellular damage and HSC activation. Our findings may open up the possibility that BNP is therapeutically applicable for the prevention of liver fibrosis.

Acknowledgments

The authors thank Mr. Hirokazu Tsujimoto and Ms. Yoshie Fukuchi for technical assistance, Dr. Naoshi Nishida for expert opinions, and Mrs. Ayumi Ishida, Ms. Shiho Takada, and Ms. Aki Egami for secretarial assistance. This work was supported by the Takeda Science Foundation, the Takeda Medical Research Foundation, the Mochida Memorial Foundation for Medical and Pharmaceutical Research, the Cell Science Research Foundation, the Japan Smoking Foundation, a Grant-in-Aid for Scientific Research from the Ministry of Education, Culture, Sports, Science and Technology, and the Research Grant for Cardiovascular Diseases (19C-7 and 20C-3) from the Ministry of Health, Labour and Welfare.

Appendix A. Supplementary data

Supplementary data associated with this article can be found, in the online version, at doi:10.1016/j.febslet.2009.05.025.

References

[1] Tamura, N. and Garbers, D.L. (2004) Guanylyl cyclase receptors in: Encyclopedia of Endocrine Diseases (Martini, L. Ed.), vol. 2, pp. 415–421, Academic Press, San Diego.
[2] Chalasani, N., Gorski, J.C., Asghar, M.S., Asghar, A., Foresman, B., Hall, S.D. and Crabb, D.W. (2003) Hepatic cytochrome P450 2E1 activity in nondiabetic patients with nonalcoholic steatohepatitis. Hepatology 37, 544–550.
[3] Wallace, K., Burt, A.D. and Wright, M.C. (2008) Liver fibrosis. Biochem. J. 411, 1–18.
[4] Bradford, B.U., Kono, H., Isayama, F., Kosyk, O., Wheeler, M.D., Akiyama, T.E., Bleye, L., Krausz, K.W., Gonzalez, F.J., Koop, D.R. and Rusyn, I. (2005) Cytochrome P450 CYP2E1, but not nicotinamide adenine dinucleotide phosphate oxidase, is required for ethanol-induced oxidative DNA damage in rodent liver. Hepatology 41, 336–344.
[5] Murakami, S., Nagaya, N., Itoh, T., Fujii, T., Iwase, T., Hamada, K., Kimura, H. and Kangawa, K. (2004) C-type natriuretic peptide attenuates bleomycin-induced pulmonary fibrosis in mice. Am. J. Physiol. Lung Cell. Mol. Physiol. 287, L1172–7.
[6] Soeki, T., Kishimoto, I., Okumura, H., Tokudome, T., Horio, T., Mori, K. and Kangawa, K. (2005) C-type natriuretic peptide, a novel antifibrotic and antihypertrophic agent, prevents cardiac remodeling after myocardial infarction. J. Am. Coll. Cardiol. 45, 608–616.
[7] Tamura, N., Ogawa, Y., Chusho, H., Nakamura, K., Nakao, K., Suda, M., Kasahara, M., Hashimoto, R., Katsuura, G., Mukoyama, M., Itoh, H., Saito, Y., Tanaka, I., Otani, H. and Katsuki, M. (2000) Cardiac fibrosis in mice lacking brain natriuretic peptide. Proc. Natl. Acad. Sci. USA 97, 4239–4244.
[8] Suganami, T., Mukoyama, M., Sugawara, A., Mori, K., Nagae, T., Kasahara, M., Yahata, K., Makino, H., Fujinaga, Y., Ogawa, Y., Tanaka, I. and Nakao, K. (2001) Overexpression of brain natriuretic peptide in mice ameliorates immune-mediated renal injury. J. Am. Soc. Nephrol. 12, 2652–2663.
[9] Ogawa, Y., Itoh, H., Tamura, N., Suga, S., Yoshimasa, T., Uehira, M., Matsuda, S., Shiono, S., Nishimoto, H. and Nakao, K. (1994) Molecular cloning of the complementary DNA and gene that encode mouse brain natriuretic peptide and generation of transgenic mice that overexpress the brain natriuretic peptide gene. J. Clin. Invest. 93, 1911–1921.
[10] Sone, M., Itoh, H., Yamahara, K., Yamashita, JK., Yurugi-Kobayashi, T., Nonoguchi, A., Suzuki, Y., Chao, T.H., Sawada, N., Fukunaga, Y., Miyashita, K., Park, K., Oyamada, N., Sawada, N., Taura, D., Tamura, N., Kondo, Y., Nito, S., Suemori, H., Nakatsuji, N., Nishikawa, S. and Nakao, K. (2007) Pathway for differentiation of human embryonic stem cells to vascular cell components and their potential for vascular regeneration. Arterioscler. Thromb. Vasc. Biol. 27, 2127–2134.
[11] Tao, J., Mallat, A., Gallois, C., Belmadani, S., Méry, P.F., Nhieu, J.T., Pavoine, C. and Lotersztajn, S. (1999) Biological effects of C-type natriuretic peptide in human myofibroblastic hepatic stellate cells. J. Biol. Chem. 274, 23761–23769.
[12] Görbig, M.N., Ginès, P., Bataller, R., Nicolás, J.M., Garcia-Ramallo, E., Tobías, E., Titos, E., Rey, M.J., Clària, J., Arroyo, V. and Rodés, J. (1999) Atrial natriuretic peptide antagonizes endothelin-induced calcium increase and cell contraction in cultured human hepatic stellate cells. Hepatology 30, 501–509.
[13] Bilzer, M., Jaeschke, H., Vollmar, A.M., Paumgartner, G. and Gerbes, A.L. (1999) Prevention of Kupffer cell-induced oxidant injury in rat liver by atrial natriuretic peptide. Am. J. Physiol. 276, G1137–G1144.

[14] Ishigaki, N., Yamamoto, N., Jin, H., Uchida, K., Terai, S. and Sakaida, I. (2009) Continuous intravenous infusion of atrial natriuretic peptide (ANP) prevented liver fibrosis in rat. Biochem. Biophys. Res. Commun. 378, 354–359.
[15] Li, Y., Kishimoto, I., Saito, Y., Harada, M., Kuwahara, K., Izumi, T., Takahashi, N., Kawakami, R., Tanimoto, K., Nakagawa, Y., Nakanishi, M., Adachi, Y., Garbers, D.L., Fukamizu, A. and Nakao, K. (2002) Guanylyl cyclase-A inhibits angiotensin II type 1A receptor-mediated cardiac remodeling, an endogenous protective mechanism in the heart. Circulation 106, 1722–1728.
[16] Yamashita, T., Tokutomi, Y., Matsuba, S., Ichijo, H., Ogawa, H. and Kim-Mitsuyama, S. (2008) Olmesartan prevents cardiovascular injury and hepatic steatosis in obesity and diabetes, accompanied by apoptosis signal regulating kinase-1 inhibition. Hypertension 52, 573–580.

Induction and Isolation of Vascular Cells From Human Induced Pluripotent Stem Cells—Brief Report

Daisuke Taura, Masakatsu Sone, Koichiro Homma, Naofumi Oyamada, Kazutoshi Takahashi, Naohisa Tamura, Shinya Yamanaka, Kazuwa Nakao

Objective—Induced pluripotent stem (iPS) cells are a novel stem cell population derived from human adult somatic cells through reprogramming using a defined set of transcription factors. Our aim was to determine the features of the directed differentiation of human iPS cells into vascular endothelial cells (ECs) and mural cells (MCs), and to compare that process with human embryonic stem (hES) cells.

Methods and Results—We previously established a system for differentiating hES cells into vascular cells. We applied this system to human iPS cells and examined their directed differentiation. After differentiation, TRA1-60$^-$ Flk1$^+$ cells emerged and divided into VE-cadherin–positive and –negative populations. The former were also positive for CD34, CD31, and eNOS and were consistent with ECs. The latter differentiated into MCs, which expressed smooth muscle α-actin and calponin after further differentiation. The efficiency of the differentiation was comparable to that of human ES cells.

Conclusions—We succeeded in inducing and isolating human vascular cells from iPS cells and indicate that the properties of human iPS cell differentiation into vascular cells are nearly identical to those of hES cells. This work will contribute to our understanding of human vascular differentiation/development and to the development of vascular regenerative medicine. (*Arterioscler Thromb Vasc Biol.* **2009;29:1100-1103.**)

Key Words: angiogenesis ■ stem cells ■ vascular biology ■ endothelium ■ differentiation

Pluripotent embryonic stem (ES) cells are thought to represent a potentially unlimited pool from which to derive cells for new treatments in the area of regenerative medicine and for investigation of cell development/differentiation. We previously described the process by which mouse, monkey and human embryonic stem (ES) cells differentiate into vascular cells.[1,2,3] In addition, we used the hindlimb ischemia model with immunodeficient mice to demonstrate that transplanted vascular endothelial cells (ECs) and mural cells (MCs) derived from human (h)ES cells could be successfully incorporated into the host vasculature and significantly accelerate improvements in local blood flow.[3,4] However, immunologic and ethical problems remain to be overcome before clinical application.

Recently, novel ES cell-like pluripotent cells were generated from mouse skin fibroblasts by introducing 4 transcription factors.[5] Termed induced pluripotent stem (iPS) cells, they were subsequently generated from human skin fibroblasts.[6,7] At present, the properties of human iPS cell differentiation into vascular cells remain unknown. To address that issue, we investigated the differentiation of human iPS cells into ECs and MCs using our differentiation system previously developed for hES cells.

Materials and Methods

Cell Culture

hES, human iPS, and OP9 feeder cells were all established and maintained as described previously.[6,8,9] To induce differentiation, hES or iPS cells were cultured on an OP9 feeder layer as described previously.[3]

Flow Cytometry and Cell Sorting

Flow cytometric analysis and cell sorting were performed as described previously.[1,9]

Immunohistochemistry

Cultured cells were stained with various monoclonal antibodies as described.[1,9]

For details regarding cell culture, RT-PCR, and the antibodies used in flow cytometry and immunohistochemistry, please see the supplemental material (available online at http://atvb.ahajournals.org).

Received December 4, 2008; revision accepted April 16, 2009.

From the Department of Medicine and Clinical Science (D.T., M.S., K.H., N.O., N.T., K.N.), Kyoto University Graduate School of Medicine; the Department of Stem Cell Biology (K.T., S.Y.), Institute for Frontier Medical Sciences, Kyoto University; and the Center for iPS Cell Research and Application (CiRA) (K.T., S.Y.), Institute for Integrated Cell-Material Sciences, Kyoto University, Japan.

Correspondence to Masakatsu Sone, MD, PhD, 54 Shogoin Kawahara-cho, Sakyo-ku, Kyoto 606-8507, Japan. E-mail sonemasa@kuhp.kyoto-u.ac.jp

Arterioscler Thromb Vasc Biol is available at http://atvb.ahajournals.org

DOI: 10.1161/ATVBAHA.108.182162

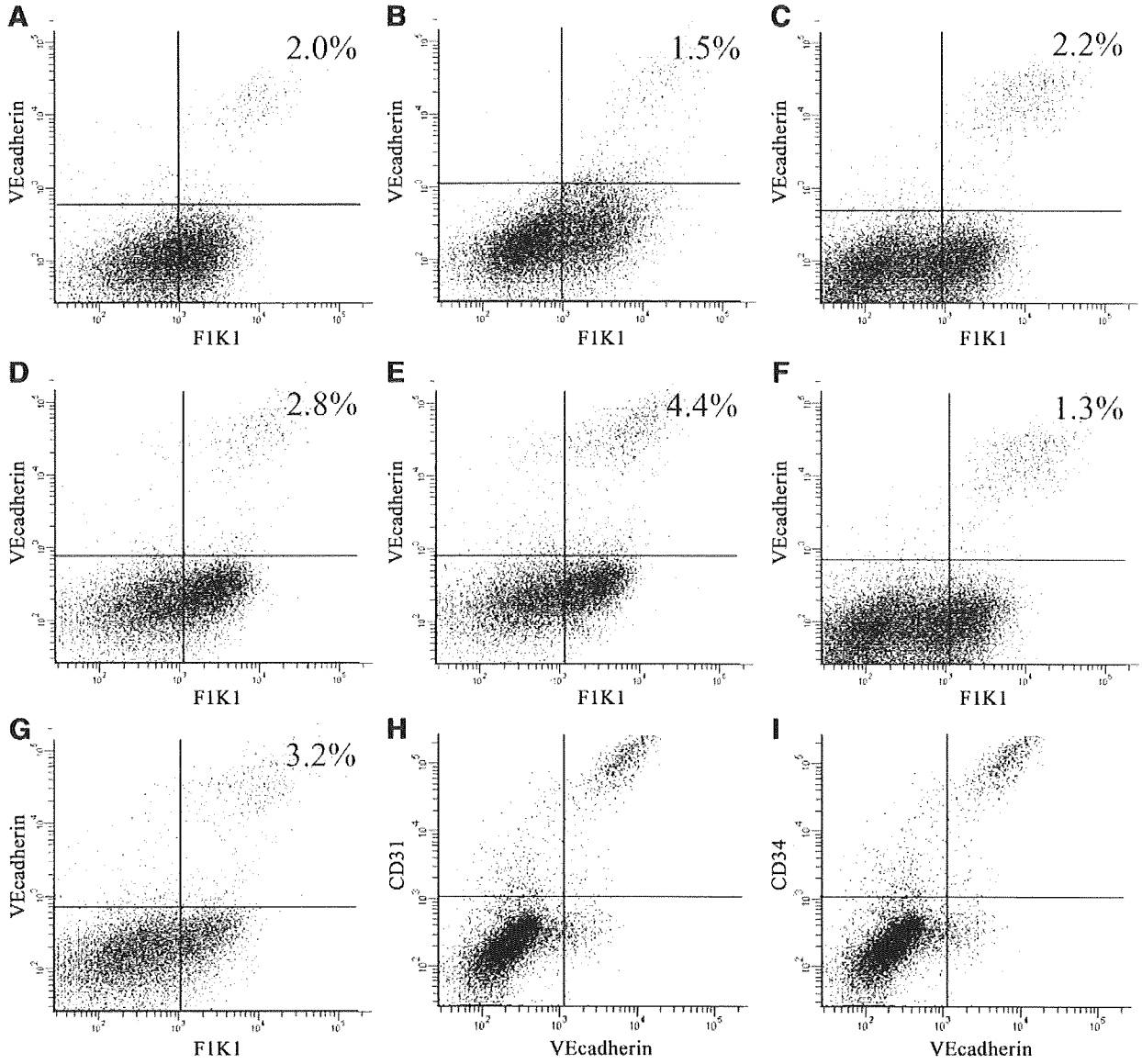

Figure 1. Flow cytometric analysis of hES-derived and iPS-derived cells on day 10 of differentiation. A through C, hES-derived cells (A, H9; B, HES3; C, KhES-1). D through G, iPS-derived cells (D, B6; E, B7; F, G1; G, G4). H and I, Analysis of human iPS-derived cells with other EC markers.

Results

We investigated 3 hES cell lines (H9, HES3, and KhES1) and 4 iPS cell lines (201B6, 201B7, 253G1, and 253G4).[5,6] 201B6 (B6) and 201B7 (B7) cells were generated from human skin fibroblasts by transfection with 4 transcription factors (Oct3/4, Sox2, Klf4, c-Myc), whereas 253G1 (G1) and 253G4 (G4) were generated using only 3 factors (c-Myc was omitted).[10] The morphology of these 4 lines did not differ from hES cells, and they were also positive for hES cell markers (supplemental Figure I). We induced differentiation of these iPS cell lines in an in vitro 2D culture system previously established for differentiation of hES cells into vascular cells.[3] After 10 days of differentiation, cells positive for Flk1 (also designated VEGF receptor-2) and the EC marker VE-cadherin emerged and accounted for 1% to 5% of the cells (Figure 1A through 1G). We noted no differences in the differentiation of the B and G lines, and both were comparable to the hES lines (Figure 1A through 1G). The $Flk1^+$ $VE\text{-}cadherin^+$ cell population was also positive for CD31 and CD34 (Figure 1H and 1I), and negative for the ES cell marker tumor rejection antigen 1–60 (TRA1–60). We sorted those cells and recultured with VEGF, and found that they formed a network-like structure on Matrigel, in vitro (Figure 2A), and had a cobblestone appearance when confluent on collagen IV-coated dishes (Figure 2B). Immunofluorescent staining for CD31 produced a characteristic marginal staining pattern (Figure 2C), and staining for endothelial NO synthase produced a cytoplasmic pattern (Figure 2D). Based on these observations, the cells were consistent with ECs. Subsequent RT-PCR analysis of EC markers revealed that both human iPS-derived and hES-derived ECs expressed

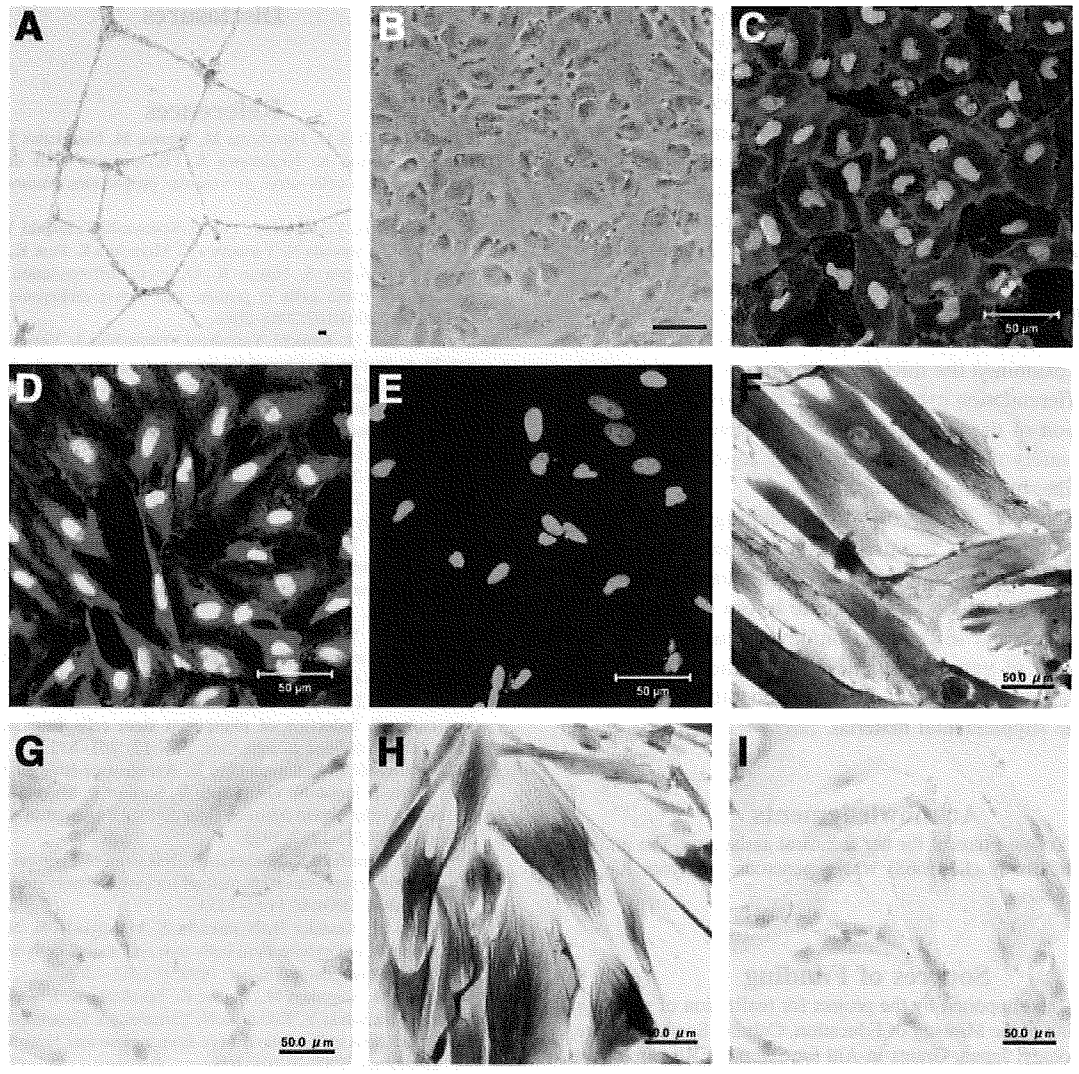

Figure 2. A, Network formation by iPS-derived VE-cadherin$^+$ cells after 24 hours of culture on Matrigel. B, Phase-contrast photomicrograph of iPS-derived VE-cadherin$^+$ cells. C through E, Immunostaining of VE-cadherin$^+$ cells: red, CD31 (C) or eNOS (D) or control mouse IgG1 (E; as negative control for C and D); green, nuclei. F through I, Immunostaining of VE-cadherin$^-$ Flk1$^+$ cells for MC markers: F, αSMA; G, control mouse IgG2 (negative control for F); H, calponin; I, control mouse IgG1 κ (negative control for H). Scale bars=50 μm.

VE-cadherin, CD31, von Willebrand factor (vWF), and CD34 at levels similar to those seen in adult ECs (supplemental Figure II).

We next sorted for Flk1$^+$ VE-cadherin$^-$ TRA1–60$^-$ cells on day 10 of differentiation and then induced differentiation into MCs using PDGF-BB as described previously.[3,4] Once differentiated, these cells stained positively for αSMA and calponin and were therefore consistent with MCs (Figure 2E and 2F). Both human iPS-derived and hES-derived MCs expressed the vascular smooth cell markers at levels similar to those seen in adult vascular smooth muscle cells (supplemental Figure II).

Discussion

The establishment of iPS cells opened a new avenue for regenerative medicine and stem cell biology. The directional differentiation of mouse iPS cells into vascular cells was recently reported.[11] In the present study, we have shown that human iPS cells can be directionally differentiated into vascular ECs and MCs by applying the same methods we established for hES cells.[3] We previously reported that the differentiation kinetics of primate ES cells to vascular cells is not equal to that of mouse ES cells.[2,3] To further clarify the differentiation process in human beings and to determine the possible clinical application of iPS cells, investigation of human iPS cells is essential because some characters were significantly different between mouse and human iPS cells as ES cells.

In contrast to human ES cells, iPS cells can be established from every human being irrespective of their genetic backgrounds. The establishment of in vitro differentiation system of human vascular cells from human iPS cells should make it possible to dissect out cellular mechanisms

in human vascular development and diseased states such as arteriosclerosis. The establishment of iPS cell lines from patients with inherited diseases presenting vascular abnormality should enable clarification of their pathogenesis. In addition, because they overcome the immunologic and ethical problems associated with human ES cells, our study should also contribute to the development of novel patient-specific cell based vascular regenerative therapies.

Several issues remain to be resolved before human iPS-derived vascular cells can be administered to humans, however. Although we observed no reappearance of undifferentiated or tumor cell-like structures in the in vitro cultures, when we examined the mRNA expression of the transgenes during differentiation experiments, we occasionally observed upregulation of the transgenic mRNA (supplemental Figure III). The safety of iPS cells needs to be confirmed for each iPS cell line, both in vitro and in vivo.

In conclusion, we succeeded in inducing and isolating human vascular cells from iPS cells and indicate that the properties of differentiation are nearly identical to those of hES cells. This work will contribute to our understanding of human vascular differentiation/development and to the development of vascular regenerative medicine.

We described additional discussions about the safety of iPS cells in the supplemental material.

Acknowledgments

We thank Yoshie Fukuchi for her technical assistance. The antihuman Flk1 antibody (KM1668) was a generous gift from Kyowa Hakko Co Ltd.

Sources of Funding

This work was supported by the project for realization of regenerative medicine of the Ministry of Education, Culture, Sports, Science, and Technology, Japan, Grants-in-Aid for Scientific Research from the Ministry of Health, Labor, and Welfare, the Ministry of Education, Culture, Sports, Science, and Technology, the Takeda Science Foundation, the Japan Cardiovascular Research Foundation, and the Smoking Research Foundation.

Disclosures

None.

References

1. Yamashita J, Itoh H, Hirashima M, Ogawa M, Nishikawa S, Yurugi T, Naito M, Nakao K, Nishikawa S. Flk1-positive cells derived from embryonic stem cells serve as vascular progenitors. *Nature*. 2000;408:92–96.
2. Sone M, Itoh H, Yamashita J, Yurugi-Kobayashi T, Suzuki Y, Kondo Y, Nonoguchi A, Sawada N, Yamahara K, Miyashita K, Park K, Shibuya M, Nito S, Nishikawa S, Nakao K. Different differentiation kinetics of vascular progenitor cells in primate and mouse embryonic stem cells. *Circulation*. 2003;107:2085–2088.
3. Sone M, Itoh H, Kenichi Yamahara, Yamashita J, Yurugi-K T, Nonoguchi A, Suzuki Y, Chao TH, Sawada N, Fukunaga Y, Miyashita K, Park K, Oyamada N, Sawada N, Taura D, Tamura N, Kondo Y, Nito S, Suemori H, Nakatsuji N, Nishikawa N, Nakao K, Pathway for differentiation of human embryonic stem cells to vascular cell components and their potential for vascular regeneration. *Arterioscler Thromb Vasc Biol*. 2007;27:2127–2134.
4. Yamahara K, Sone M, Itoh H, Yamashita J, Yurugi-K T, Homma K, Chao TH, Miyashita K, Park K, Oyamada N, Sawada N, Taura D, Fukunaga Y, Tamura N, Nakao K. Augmentation of Neovascularizaition in hindlimb ischemia by combined transplantation of human embryonic stem cells-derived endothelial and mural cells. *PLOS one*. 2008;3:e1666.
5. Takahashi K, Yamanaka S. Induction of pluripotent stem cells from mouse embryonic and adult fibroblast cultures by defined factors. *Cell*. 2006;126:663–676.
6. Takahashi K, Tanabe K, Ohnuki M, Narita M, Ichisaka T, Tomoda K, Yamanaka S. Induction of pluripotent stem cells from adult human fibroblasts by defined factors. *Cell*. 2007;131:861–872.
7. Yu J, Vodyanik MA, Smuga-Otto K, Antosiewicz-Bourget J, Frane JL, Tian S, Nie J, Jonsdottir GA, Ruotti V, Stewart R, Slukvin II, Thomson JA. Induced pluripotent stem cell lines derived from human somatic cells. *Science*. 2007;318:1917–1920.
8. Fujioka T, Yasuchika K, Nakamura Y, Nakatsuji N, Suemori H. A simple and efficient cryopreservation method for primate embryonic stem cells. *Int J Dev Biol*. 2004;48:1149–1154.
9. Hirashima M, Kataoka H, Nishikawa S, Matsuyoshi N, Nishikawa S. Maturation of embryonic stem cells into endothelial cells in an in vitro model of vasculogenesis. *Blood*. 1999;93:1253–1263.
10. Nakagawa M, Koyanagi M, Tanabe K, Takahashi K, Ichisaka T, Aoi T, Okita K, Mochiduki Y, Takizawa N, Yamanaka S. Generation of induced pluripotent stem cells without Myc from mouse and human fibroblasts. *Nat Biotechnol*. 2008;26:101–106.
11. Narazaki G, Uosaki H, Teranishi M, Okita K, Kim B, Matsuoka S, Yamanaka S, Yamashita J. Directed and systematic differentiation of cardiovascular cells from mouse induced pluripotent stem cells. *Circulation*. 2008;118:498–506.

Guanylyl Cyclase-A Inhibits Angiotensin II Type 2 Receptor-Mediated Pro-Hypertrophic Signaling in the Heart

Yuhao Li, Yoshihiko Saito, Koichiro Kuwahara, Xianglu Rong, Ichiro Kishimoto, Masaki Harada, Yuichiro Adachi, Michio Nakanishi, Hideyuki Kinoshita, Masatsugu Horiuchi, Michael Murray, and Kazuwa Nakao

Department of Medicine and Clinical Science (Y.L., K.K., X.R., M.H., Y.A., M.N., H.K., K.N.), Kyoto University Graduate School of Medicine, Kyoto 606-8507, Japan; First Department of Internal Medicine (Y.S.), Nara Medical University, Nara 634, Japan; National Cardiovascular Center Research Institute (I.K.), Osaka 565-8565, Japan; Department of Molecular Cardiovascular Biology and Pharmacology (M.H.), Ehime University Graduate School of Medicine, Ehime 791-0295, Japan; and Faculty of Pharmacy (M.M.), The University of Sydney, Sydney, New South Wales 2006, Australia

Angiotensin II plays a key role in the development of cardiac hypertrophy. The contribution of the angiotensin II type 1 receptor (AT1) in angiotensin II-induced cardiac hypertrophy is well established, but the role of AT2 signaling remains controversial. Previously, we have shown that natriuretic peptide receptor/guanylyl cyclase-A (GCA) signaling protects the heart from hypertrophy at least in part by inhibiting AT1-mediated pro-hypertrophic signaling. Here, we investigated the role of AT2 in cardiac hypertrophy observed in mice lacking GCA. Real-time RT-PCR and immunoblotting approaches indicated that the cardiac AT2 gene was overexpressed in GCA-deficient mice. Mice lacking AT2 alone did not exhibit an abnormal cardiac phenotype. In contrast, GCA-deficiency-induced increases in heart to body weight ratio, cardiomyocyte cross-sectional area, and collagen accumulation as evidenced by van Gieson staining were attenuated when AT2 was absent. Furthermore, the up-regulated cardiac expression of hypertrophy-related genes in GCA-null animals was also suppressed. Pharmacological blockade of AT2 with PD123319 similarly attenuated cardiac hypertrophy in GCA-deficient mice. In addition, whereas the AT1 antagonist olmesartan attenuated cardiac hypertrophy in GCA-deficient mice, this treatment was without effect on cardiac hypertrophy in GCA/AT2-double null mice, notwithstanding its potent antihypertensive effect in these animals. These results suggest that the interplay of AT2 and AT1 may be important in the development of cardiac hypertrophy. Collectively, our findings support the assertion that GCA inhibits AT2-mediated pro-hypertrophic signaling in heart and offer new insights into endogenous cardioprotective mechanisms during disease pathogenesis. (***Endocrinology*** **150: 3759–3765, 2009)**

Cardiac hypertrophy is an independent risk factor for cardiac morbidity and mortality. Left ventricular hypertrophy is a major, independent predictor of cardiovascular events, particularly in hypertension, in which it dramatically increases the risk of stroke, coronary heart disease, and heart failure (1). Therefore, elucidation of the underlying mechanism leading to cardiac hypertrophy may have significant implications for the development of therapeutic strategies.

Atrial natriuretic peptide (ANP) is a cardiac hormone that acts through guanylate cyclase-A (GCA) to lower blood pressure and dilate blood vessels *in vivo* (2) and to inhibit the growth of cardiac myocytes and fibroblasts *in vitro* (3). Brain natriuretic peptide (BNP) also activates GCA and has effects similar to those of ANP, although it also exerts local antifibrotic actions in the ventricle (4). Mice lacking GCA exhibit hypertension, cardiac hypertrophy, and fibrosis and are prone to sudden death, which is consistent with a protective role for natriuretic peptide/GCA-signaling pathways in the cardiovascular system (5–8).

Angiotensin (Ang) II plays a key role in the development of cardiac hypertrophy (9). Although most of the cardiovascular

ISSN Print 0013-7227 ISSN Online 1945-7170
Printed in U.S.A.

doi: 10.1210/en.2008-1353 Received September 18, 2008. Accepted April 6, 2009.
First Published Online April 16, 2009

Abbreviations: ACE, Angiotensin converting enzyme; Agt, angiotensinogen; Ang, angiotensin; ANP, atrial natriuretic peptide; AT1, angiotensin II type 1 receptor; BNP, brain natriuretic peptide; BW, body weight; GCA, guanylyl cyclase-A; HW, heart weight; KO, knockout; LVW, left ventricular weight; NPR, natriuretic peptide receptor; RVW, right ventricular weight; SBP, systolic blood pressure; WT, wild type.

effects of Ang II are mediated via the Ang II type 1 receptor (AT1) (10), the alternate major Ang II receptor subtype, AT2, may also be important because its expression is up-regulated in cardiovascular pathologies, including cardiac hypertrophy (11, 12) and heart failure (13). Although the roles of AT2 in cardiac remodeling remain controversial, accumulating lines of evidence appear to support the view that AT2 can promote cardiac growth in pathological situations. Indeed, at least in some tissues, AT1 and AT2 share common signaling pathways that stimulate cell and tissue proliferation (14–18).

We have demonstrated previously that genetic or pharmacological blockade of AT1a signaling attenuates cardiac hypertrophy and fibrosis in GCA-deficient mice (6, 7), suggesting that GCA inhibits AT1a-mediated pathological signaling in the heart. Importantly, however, the cardiac hypertrophy and fibrosis in GCA-deficient mice was not completely abolished in animals lacking both GCA and AT1a (6). Similarly, AT1 blockade by olmesartan (CS-866) in GCA-null mice only partially reversed the increase in cardiac hypertrophy and fibrosis, suggesting the involvement of AT1-independent signaling in cardiac remodeling observed in GCA-deficient mice. In the present study, we investigated the role played by AT2 in cardiac hypertrophy induced by GCA deficiency using further genetic and pharmacological manipulation in mice. The findings of this study are consistent with a pro-hypertrophic effect of AT2 signaling in heart.

Materials and Methods

Animals and treatments

All experimental procedures were performed according to Kyoto University standards for animal care.

Experiment 1

Male homozygous GCA-deficient [$GCA^{-/-}/AT2^{+/y}$, GCA knockout (KO)] and wild-type (WT, $GCA^{+/+}/AT2^{+/y}$) mice used in this experiment (n = 7 each group) were generated by methods described previously (5). The genetic backgrounds of the mice were C57BL/6. Animals at 16–17 wk of age were killed for initial gene analysis.

Experiment 2

The genetic backgrounds of the AT2-deficient ($GCA^{+/+}/AT2^{-/y}$, AT2 KO) mice were FVB/N. Male homozygous AT2 KO, GCA KO, $GCA^{-/-}/AT2^{-/y}$ (double KO), and WT mice used in this experiment (n = 7–9 each group) were generated from the heterozygotes after crossing female AT2 KO and male GCA KO mice. Systolic blood pressure (SBP) was measured at 11, 14, and 16 wk of age using a noninvasive computerized tail-cuff method (BP98A; Softron Co., Ltd., Tokyo, Japan) (6–8). Animals at 16–17 wk of age were killed for further examination.

Experiment 3

WT and GCA KO mice were used in this experiment (n = 5 each group). The AT2 antagonist PD123319 (30 mg/kg · d; Sigma, Osaka, Japan) was dissolved in saline and administered daily by ip injection for 4 wk, in mice at 12–13 wk of age. The corresponding control animals were treated with saline only. SBP was measured before and 2 and 3 wk after treatment with the antagonist or saline using a tail-cuff method (MK-2000ST; Muromachi Kikai Co. Ltd., Tokyo, Japan). Animals were killed for further examination after 4 wk treatment.

Experiment 4

All four genotypes were used in this experiment (n = 7–9 each group). The AT1 antagonist olmesartan (a gift from Daiichi-Sankyo Co. Ltd., Tokyo, Japan) was suspended in 5% gum arabic and administered by oral gavage at a dose of 10 mg/kg once a day for 4 wk in mice at 12–13 wk of age; control animals received vehicle alone. SBP was measured 3 wk after treatment with the antagonist or vehicle using a tail-cuff method (BP98A; Softron). Animals were killed for further examination after 4 wk treatment.

Determination of heart weight (HW) and right and left ventricular weights (RVW and LVW)

Animals were euthanized, hearts were removed and weighed, and then the right and left ventricles were weighed separately. The ratios of these weights to the total body weight (BW) (HW/BW, RVW/BW, and LVW/BW) were calculated as indexes of cardiac hypertrophy.

Measurement of cardiomyocyte cross-sectional area and histological assessment of cardiac fibrosis

A segment of the excised left ventricle from each animal was fixed in 10% neutral formalin over several days and then dehydrated with graded concentrations of alcohol before embedding in paraffin. Paraffin slices from each heart were stained with hematoxylin-eosin. Morphometry of each section was performed to determine the myocyte cross-sectional area as described previously (19). The cross-sectional area of cardiomyocytes in sections that had been cut transversely was measured using a KS400 Imaging System (Carl Zeiss Vision, Eching, Germany); cardiomyocytes possessed an intact cellular membrane, and the nucleus was visible. The outer borders of the cardiomyocytes were traced at × 400 magnification, and the cardiomyocyte areas were calculated. One hundred cells per heart were counted, and the mean value was used in subsequent analyses.

To determine the extent of collagen fiber accumulation, paraffin slices from each heart were subjected to van Gieson staining. Forty fields from three individual sections were selected at random, and the van Gieson-stained areas were measured in relation to the total left ventricular area using image analysis software and a Zeiss KS400 system (6, 7).

Analysis of mRNA

Total RNA was prepared from individual left ventricles of mouse hearts using TRIzol (Life Technologies Inc., Rockville, MD). mRNAs were quantified by real-time RT-PCR using the TaqMan system (ABI PRISM 7700 Sequence Detector; Applied Biosystems, Foster City, CA) (6). The primers and probes of the genes examined were as follows: ANP sense 5′-GCCATATTGGAGCAAATCCT-3′, antisense 5′-GCAGGTTCTTGAAATCCATCA-3′, and oligonucleotide probe, 5′-TGTACAGTGCGGTGTCCAACACAGAT-3′; BNP sense 5′-CCAGTCTCCAGAGCAATTCAA-3′, antisense 5′-GCCATTTCCTCCGACTTTT-3′, and oligonucleotide probe 5′-TGCAGAAGCTGCTGGAGCTGATAAGA-3′; collagen I sense 5′-GTCCCAACCCCCAAAGAC-3′, antisense 5′-CATCTTCTGAGTTTGGTGATACGT-3′, and oligonucleotide probe 5′-CACGGCTGTGTGCGATGACG-3′; collagen III sense 5′-TGGTTTCTTCTCACCCTTCTTC-3′, antisense 5′-TGCATCCCAATTCATCTACGT-3′, and oligonucleotide probe 5′-TCCCACTCTTATTTTGGCACAGCAGTC-3′; angiotensinogen (Agt) sense 5′-CATTGGTGACACCAACCCC-3′, antisense 5′-GCTGTTCCTCCTCTCCTGCT-3′, and oligonucleotide probe 5′-AGGTTCTCAATAGCATCCTCCTCGAACTC-3′; angiotensin converting enzyme (ACE) sense 5′-CGGAATGAAACCCATTTTGA-3′, antisense 5′-GCACAAAGCTCACGAAGTACC-3′, and oligonucleotide probe 5′-CACATCCCAAACGTGACACCGTACAT-3′; AT1a sense 5′-GTTTGCGCTTTTCATTACGAGT-3′, antisense 5′-TCTTGGTTAGGCCCAGTCCT-3′, and oligonucleotide probe 5′-CCGGAATTCAACGCTCCCCA-3′; AT2 sense 5′-CCACCA GCAGAAACATTACC-3′, antisense 5′-GGACTCATTGGTGCCAGTT-3′, and oligonucleotide probe 5′-CAGCCGTCCTTTTGATAATCTCAACG-3′; and TGF-β1 sense 5′-GACGTCACTGGAGTTGTACGG-3′, antisense 5′-GCTGA-

ATCGAAAGCCCTGT-3′, and oligonucleotide probe 5′-AGCGCATC-GAAGCCATCCG −3′. Glyceraldehyde-3-phosphate dehydrogenase (housekeeping gene) mRNA was also amplified with specific primers and probe (Applied Biosystems).

Immunoblotting

AT2 protein was estimated by Western blotting (20). Total proteins were resolved on 4–12% polyacrylamide gradient gels (Invitrogen, Carlsbad, CA), electrophoretically transferred to polyvinylidene difluoride membranes, blocked [in buffer containing 20 mM Tris (pH 7.5), 150 mM NaCl, 5% BSA, 0.1% Tween 20], and incubated for 18 h at 4 C with AT2 receptor-specific antibody (Santa Cruz Biotechnology, Santa Cruz, CA). Detection was performed with peroxidase-conjugated secondary antibody, using an ECL chemiluminescence kit (Amersham, Buckinghamshire, UK). Immunoblotting with a monoclonal anti-β-actin antibody (Cell Signaling, Beverly, MA) was conducted to ensure equal protein loading.

Statistical analysis

All results are expressed as means ± SEM of values obtained in individual animals. Data were analyzed by single-factor ANOVA. If a significant effect was found, the Fisher's protected least significant difference test was performed to isolate the difference between the groups. Student's *t* test was used to assess the effect of olmesartan treatment on the hypertrophic phenotype in GCA KO mice (see Fig. 6). A value of $P < 0.05$ was considered to be statistically significant.

Results

AT2 deficiency ameliorates cardiac hypertrophy in GCA-deficient mice

We first determined cardiac gene expression of AT2 and AT1a in WT and GCA KO mice using real-time RT-PCR analysis. The results demonstrated an increase in cardiac AT2 mRNA expression in GCA-deficient mice compared with WT controls (Fig. 1A). Western blot analysis confirmed the increase in AT2 expression in GCA-null mouse heart at the protein level (Fig. 1B). In contrast, cardiac AT1a mRNA expression did not differ between WT and GCA null mice (Fig. 1C). There were no differences in the cardiac expression of Agt and ACE between WT and GCA-KO (data not shown).

To evaluate the potential role of AT2 in cardiac hypertrophy induced by GCA deficiency, we generated mice lacking both GCA and AT2 by crossing AT2 KO and GCA KO mice. There was no significant difference in BW among the four genotypes (WT, 34.1 ± 1.1 g; AT2 KO, 34.3 ± 1.1 g; GCA KO, 35.4 ± 1.1 g; double KO, 34.3 ± 0.7 g). In accord with previous reports (15, 16, 21), single deletion of AT2 did not induce a change in cardiac phenotype (Figs. 2, A–D, and 3, A, B, D, and H). By contrast, deletion of GCA alone increased SBP (Fig. 2A), HW/BW (Fig. 2B), LVW/BW (Fig. 2C), RVW/BW (Fig. 2D), the cross-sectional area of cardiomyocytes (Fig. 3, A and E), and cardiac interstitial van Gieson-staining area (Fig. 3, B and I). Importantly, SBP was not different between GCA KO and double KO mice (Fig. 2A), whereas HW/BW, LVW/BW, and RVW/BW ratios, the cross-sectional area of cardiomyocytes, and left ventricular interstitial fibrosis were all lower in double KO mice compared with GCA KO animals (Figs. 2, B–D, and 3, A, B, F, and J).

We further examined the expression of hypertrophy-related genes. Cardiomyocytes are the major source of ANP and BNP (2), which are two important molecular markers of cardiomyocyte hypertrophy (22). Collagens I and III are the principal collagen genes expressed in heart. Consistent with the changes in cardiac hypertrophy and fibrosis, deletion of AT2 alone did not alter cardiac expression of mRNAs for ANP, BNP, and collagens I and III in mice (Fig. 4, A–D). However, the increased cardiac expression of each of these genes that was observed in mice that lacked GCA was suppressed when AT2 was also deleted (Fig. 4, A–D).

To investigate the underlying mechanism, we further examined cardiac expression of Agt, ACE, AT1a, and TGF-β1 mRNAs. No differences in the expression of Agt, ACE, and AT1a mRNAs were observed between genotypes (Fig. 4, E–G). Single

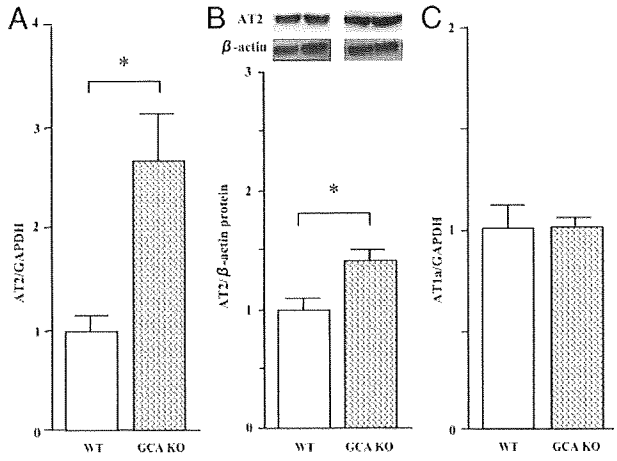

FIG. 1. Cardiac AT2, but not AT1a, is up-regulated in GCA KO mice. Total RNA was extracted from the left ventricular tissues using TRIzol. A and C, AT2 (A) and AT1a (C) mRNAs were determined by real-time RT-PCR, and the results were normalized to GAPDH. B, AT2 protein was detected by Western immunoblot analysis. Values are means ± SEM (n = 7). *, $P < 0.05$.

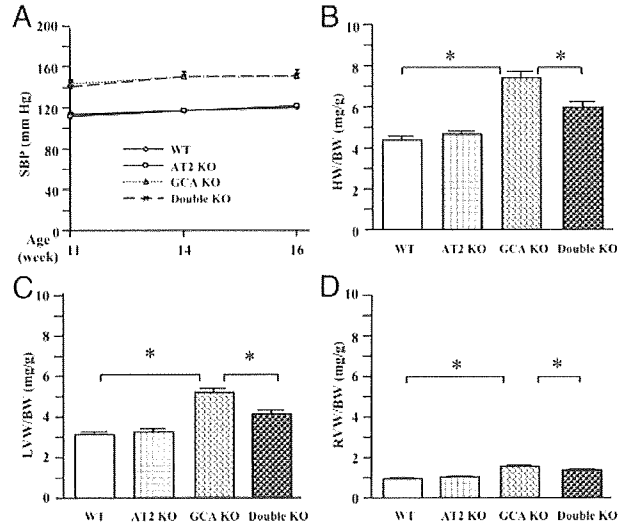

FIG. 2. Targeted deletion of AT2 ameliorated cardiac hypertrophy in GCA-deficient mice. A–D, SBP (A), HW/BW (B), LVW/BW (C), and RVW/BW (D) in WT, AT2 KO, GCA KO, and AT2/GCA double KO mice. Values are means ± SEM (n = 7–9). *, $P < 0.05$.

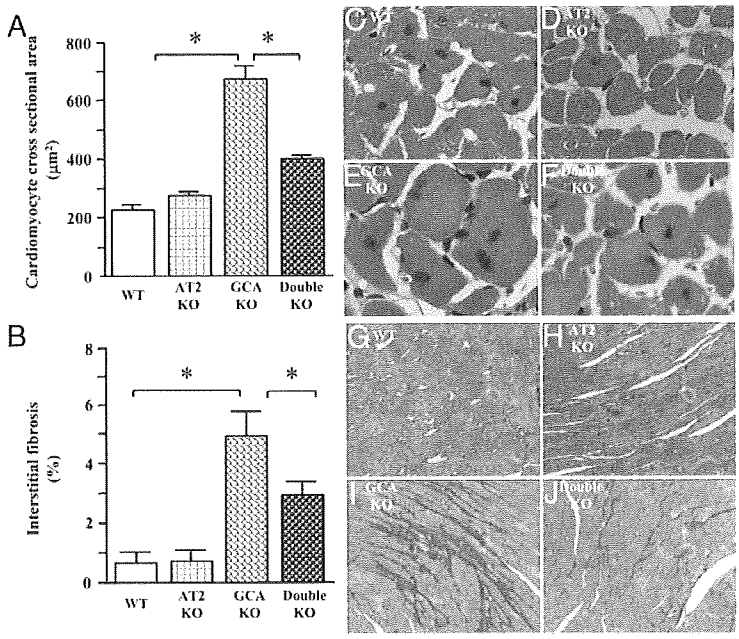

FIG. 3. Deletion of AT2 decreased cardiomyocyte cross-sectional areas and cardiac interstitial fibrosis in GCA-deficient mice. Morphometry of left ventricular myocytes was performed to measure the myocyte cross-sectional area as described previously (19). The van Gieson-stained collagen deposit area and total ventricular area in the left ventricles were analyzed using an image analyzing system. A, Cardiomyocyte cross-sectional areas in the four mouse genotypes under investigation; B, interstitial fibrosis (percent, the van Gieson-stained area to total ventricular area ratio); C–F, representative histological findings of cardiomyocytes in different experimental groups (hematoxylin-eosin staining). Magnification, ×400. G–J, Representative examples of cardiac interstitial fibrosis (*red*; ×200). Values are means ± SEM (n = 7–9). *, $P < 0.05$.

deletion of AT2 did not alter cardiac expression of TGF-β1 (Fig. 4H). However, TGF-β1 gene expression was significantly up-regulated in cardiac tissues from GCA KO mice. Consistent with the observed attenuation of cardiac hypertrophy and fibrosis, TGF-β1 expression in double KO mice was returned to the levels observed in hearts from WT mice.

Pharmacological blockade of AT2 also attenuates cardiac hypertrophy in GCA-deficient mice

To substantiate the role of AT2 in GCA deficiency-induced cardiac hypertrophy, we administered the AT2 antagonist PD123319 to GCA-null mice. Consistent with genetic blockade of AT2, PD123319 treatment for 4 wk did not affect SBP (Fig. 5A) but decreased the ratios of HW/BW and LVW/BW in GCA KO mice (Fig. 5, B and C); RVW/BW ratio was unchanged (Fig. 5D).

Residual cardiac hypertrophy in double KO mice is resistant to an AT1 antagonist

Pharmacological or genetic blockade of AT1 has been shown to attenuate GCA-deficiency-induced cardiac hypertrophy (6). Although cardiac mass in double KO mice was significantly lower than in GCA KO mice, it was still greater than that in WT and AT2 KO mice (Fig. 2, B–D). To test whether the residual hypertrophic effect might be mediated by AT1, we administered the AT1 antagonist olmesartan to WT, AT2 KO, GCA KO, and double KO mice. Olmesartan treatment similarly decreased SBP in all four of the murine genotypes under investigation (Fig. 6A). However, whereas this treatment significantly reduced HW/BW (Fig. 6B) and LVW/BW (Fig. 6C) in GCA KO, it was without effect in double KO mice.

Discussion

The role of AT2-mediated signaling pathways in the development of cardiac hypertrophy remains controversial. Initially, AT2 was reported to exert opposing effects on growth-promoting signaling mediated by AT1 (23). On the other hand, there are several reports that AT2 activates pro-hypertrophic signaling in some animal models (15, 16, 18). Thus, AT2 may have complex effects in the development of cardiovascular hypertrophy (24). It has been reported that the expression of AT2, but not AT1, is directly correlated with left ventricular mass in aortic-banded rats that exhibit cardiac hypertrophy (11, 25). In accord with these reports, the present findings from real-time RT-PCR and immunoblot analyses demonstrated that AT2, but not AT1a, was up-regulated in GCA KO mouse heart. Although deletion of AT2 alone did not induce a change in cardiac phenotype, the increase in cardiac mass reflected by increased ratios

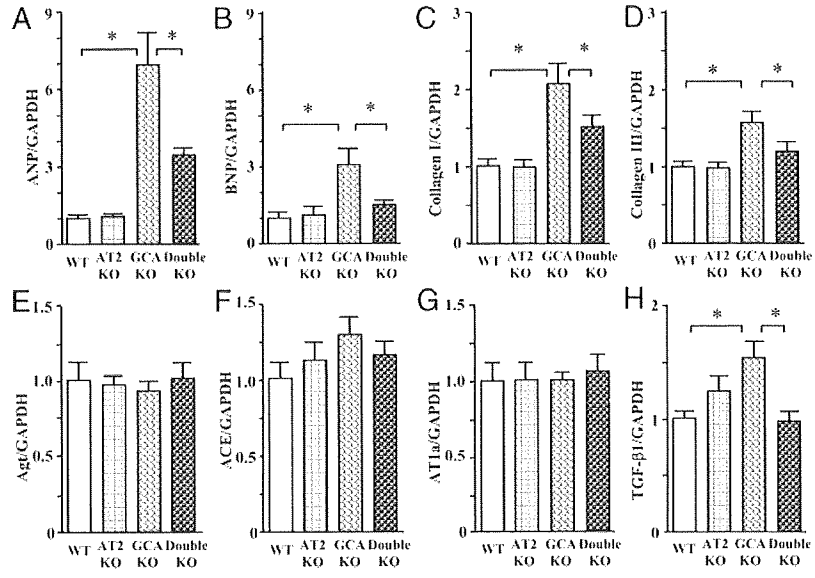

FIG. 4. Cardiac mRNA expression of the ANP (A), BNP (B), collagen I (C), collagen III (D), Agt (E), ACE (F), AT1a (G), and TGF-β1 (H) genes among different mouse genotypes. Total RNA was extracted from the left ventricular tissues using TRIzol. The relative levels of specific mRNAs were determined by real-time RT-PCR. Results were normalized to GAPDH. Values are means ± SEM (n = 7–9). *, $P < 0.05$.